ACS OMEGA

Open Access

http://pubs.acs.org/journal/acsodf

Article

Semisynthesis of Novel Alicyclic Triterpene-Triazole Derivatives from *Boswellia sacra* Gum Resin: Potential Anti-breast Cancer and Immunomodulatory Effects on T-Cell Activation

Najeeb Ur Rehman, Hassan Moghtaderi, Saeed Mohammadi, Sadiq Noor Khan, Sobia Ahsan Halim, Muhammad U. Anwar, Shaikh Mizanoor Rahman, Simon Gibbons, René Csuk, Satya Kumar Avula,* and Ahmed Al-Harrasi*

Cite This: *ACS Omega* 2025, 10, 21715−21730

Read Online

ACCESS | Metrics & More | Article Recommendations | Supporting Information

ABSTRACT: In this current work, we report on the design, synthesis, cytotoxicity of new compounds, molecular docking studies, and *in vitro* and *in silico* evaluations of 24 new alicyclic triterpene amide-containing 1*H*-1,2,3-triazole derivatives (**4**, **5**, **7a-7k** and **8a−8k**). All new compounds were characterized by ^{1}H-, ^{13}C-, ^{19}F-NMR, and HR-ESI-MS spectroscopic techniques. X-ray crystallography unambiguously confirmed the exact structure of **4**. The antibreast cancer activity of all compounds was evaluated against two prominent human breast and one normal cancer cell lines with IC_{50} values ranging from 352.31 to 61.47 μM (MDA-MB-231), 386.61 to 67.02 μM (MCF-7), and 445.37 to 103.41 μM (HDF), respectively. Eight derivatives (**7b−7i**) exhibited greater antiproliferative activities than the β-KBA (**2**) used as a reference compound. Compound **7f** demonstrated noteworthy activity even at lower concentrations. In contrast, compounds **8a** and **8k** demonstrated relatively lower effects, being compared with parent compound **2**. Furthermore, compound **7f** significantly expanded CD4+ CD8- helper T cell population at both 5 and 10 μM concentrations, increasing the expression of PD-1 and TIGIT immune checkpoints at 5 μM. The binding modes of the most active hits (**7b−7i**) were deduced by in silico docking using cyclin-dependent kinase 4 (CDK4) as a prominent target. The molecular docking studies demonstrated appreciable binding interactions and docking scores of compounds at CDK-4 ligand binding site and a significant role for −OH in compound **2** and the amide linker and triazole moiety in the binding of these compounds.

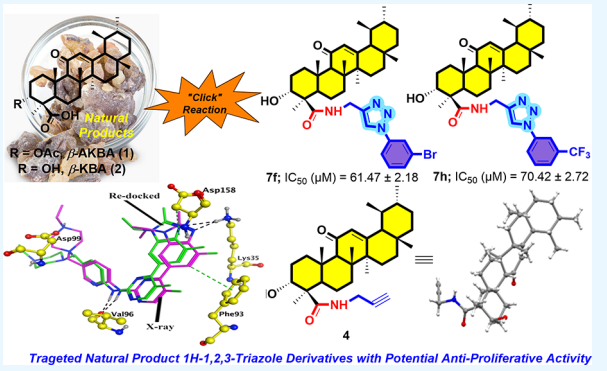

1. INTRODUCTION

Cancer, a multistage progressive disease, is one the leading causes of death after heart disease.[1] According to the World Health Organization (WHO), cancer is the second leading cause of death around the world, contributing to approximately 9.6 million deaths in 2018.[2] In both males and females, lung cancer has the greatest incidence rate (11.6% of total cases), followed by female breast cancer (11.6%) and colorectal cancer (10.2%). Among them, three cancers also rank among the top five in terms of cancer mortality (lung, 18.4%; colorectal, 9.2%; breast, 6.6% of all cancer deaths).[3] Breast cancer (BC) is the most common type in women, and its incidence increases every year.[4] It is classified into three main subgroups, determined by the existence or absence of human epidermal growth factor 2 (HER2), hormone receptors (HR), and one of the subtypes is triple-negative breast cancer (TNBC).[5] Because of the mortality and increased chance of sickness recurrence, TNBC patients require a specialized approach to highly effective and targeted medications.[6−11] Recently, TNBC management is challenging due to a lack of targeted therapies. To address this issue, it is critical to identify new antibreast compounds with low toxicity, safe and easily available.

Boswellic acids (BAs), naturally occurring well-known triterpene acids, are mostly isolated from the gum resin of the *Boswellia* species (frankincense).[12,13] Notably, derivatives of BAs, especially 3-O-acetyl-11-keto-β-boswellic acid (β-AKBA, **1**) and 11-oxo-β-boswellic acid (β-KBA, **2**), have gained much interest due to their different cytotoxic activities and their ability to induce apoptosis in breast cancer, glioblastoma, and prostate cancers cells.[4,14,15] These natural compounds are widely acknowledged for their wide range of pharmacological proper-

Received: February 10, 2025
Revised: March 19, 2025
Accepted: March 26, 2025
Published: May 22, 2025

Scheme 1. Gram-Scale Production of Natural Products of β-AKBA (1) and β-KBA (2) Isolated from *Boswellia sacra* Gum Resin[a]

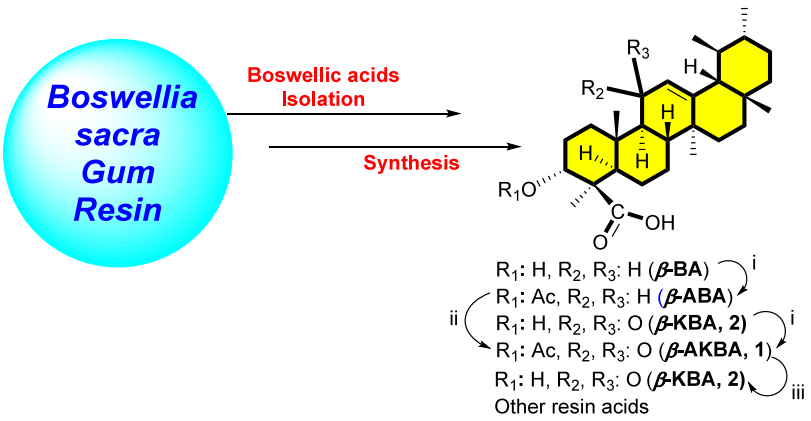

[a]Scheme 1: Reagents and conditions: (i) Ac_2O/Py/DMAP, DCM, room temperature, 6 h; (ii) NBS/$CaCO_3$/H_2O/hν, dioxane, room temperature, 10 h; (iii) 0.5 N KOH in ^{i}PrOH, reflux, 10 h.

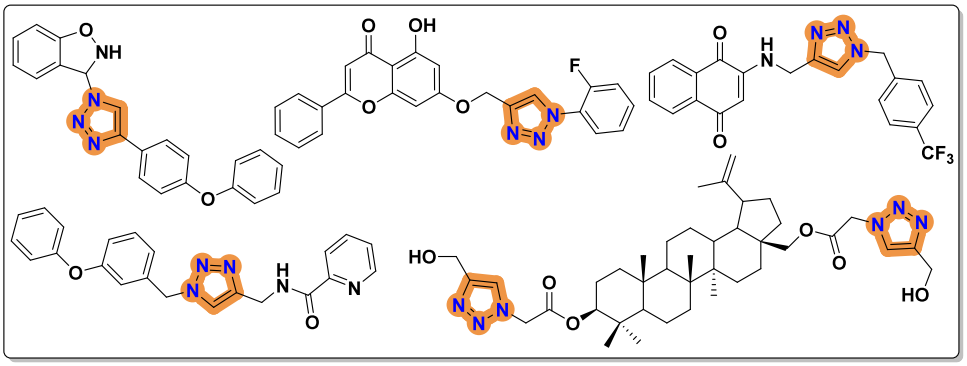

Figure 1. Representative analogues of 1*H*-1,2,3-triazoles with anticancer and antiproliferative activities.

ties, which include anti-inflammatory, cytotoxic, antiapoptotic, antiproliferative, and even therapeutic activity in the treatment of brain cancers.[15,16] The in vivo cytotoxic activity of BAs against numerous cancers, including prostate cancer,[17] colorectal cancer,[18] leukemia,[19] colon cancer,[20] Ehrlich tumor,[21] glioma,[22] and pancreatic cancer[23] are documented in the literature.

Notably, there are few clinical trials reporting the successful use of BAs for the treatment of cancer, including brain, breast and lung cancer.[24−28] Previously, we reported some derivatives of β-KBA that induced apoptosis in breast and prostate cancers cells.[29] Similarly, Csuk et al. (2015) determined the effect of β-KBA and its derivatives on breast and cervical cancer cells.[30] We also discovered the antiproliferative activity of new synthetic boswellic acid derivatives.[31] Recently, our group reported the cytotoxicity, apoptotic, and epigenetic effects of BA derivatives against breast (MCF-7, and MDA-MB-231) and normal cell lines (MCF-10A).[14] The same group determined the anticancer activity against melanoma cells using a 3-*O*-acetyl-β-boswellic acid-loaded 3D printed scaffold.[32] Our recent investigations revealed that 3-O-acetyl-11-keto-β-boswellic acid and β-BA could inhibit T cell proliferation and activation without inducing cytotoxicity.[33]

According to the previously published protocol,[34,35] the β-AKBA (**1**) and β-ABA concentration increased in the resins (30 g) of *B. sacra* and purified through column chromatography. β-AKBA (**1**) (4.5 g) was then deacetylated to β-KBA (**2**) (3.8 g) using 1N KOH in ^{i}ProH, reflux for 6 h at 80−85 °C (Scheme 1).[36]

According to the literature, structures comprising 1*H*-1,2,3-triazoles are usually regarded as significant building blocks, linkers, and have bioisosteric effects, which are believed to be related to their similarity to amide-bonds in terms of distance and planarity. Many bioactive scaffolds and therapeutic structures have 1*H*-1,2,3-triazole cores, which have anticancer, anti-HIV, antiviral, and antibacterial effects. The 1*H*-1,2,3-triazole ring system can be found in hundreds of United States Food and Drug Administration (FDA) authorized pharmaceuticals that are on the market, some of which are represented in Figure 1.[37]

Recently, we synthesized a series of new analogues of 3-*O*-acetyl-11-keto-β-boswellic acid (β-AKBA), 3-*O*-acetyl-β-boswellic acid (β-ABA) and 1*H*-1,2,3-triazole hybrids of β-AKBA through a highly efficient *"click"* chemistry reaction protocol. Among them, three compounds exhibited noteworthy inhibition, several times more potent than the parent compounds (Figure 2).[38]

In view of the above findings and in continuation of our interest in the exploration of novel antibreast cancer drugs, the present work was designed to synthesize β-KBA in bulk amounts and then a variety of novel β-KBA skeleton based 1*H*-1,2,3-triazole derivatives (**7a-7k** and **8a-8k**) were synthesized and further evaluated against antibreast cancer (MDA-MB-231, MCF-7) cell lines as well as normal human dermal cells (HDF).

2. RESULTS AND DISCUSSION

2.1. Chemistry. *2.1.1. Synthesis of Novel Alicyclic Triterpene Amide Containing 1H-1,2,3-Triazole Derivatives.*

https://doi.org/10.1021/acsomega.5c01259
ACS Omega 2025, 10, 21715−21730

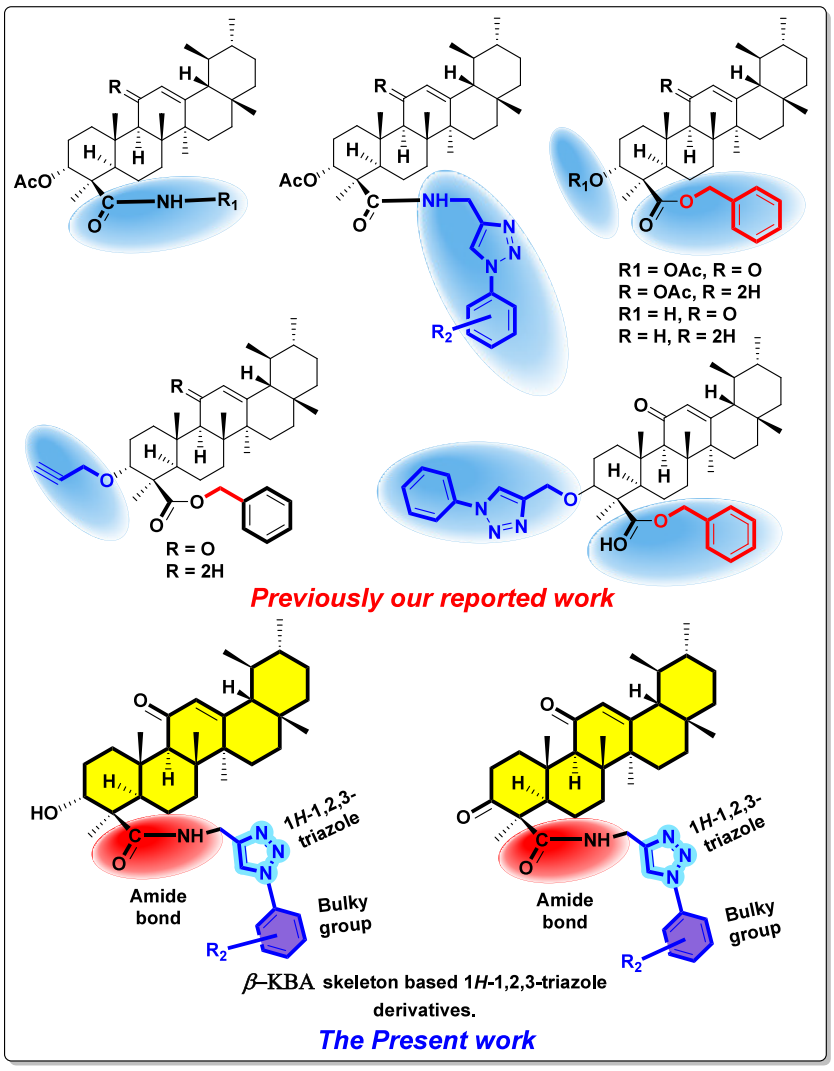

Figure 2. Structures of some derivatives of BAs with their antibreast cancer activity.

In the current study, the synthetic scheme of the *β*-KBA skeleton based 1*H*-1,2,3-triazole derivatives (**7a-7k** and **8a-8k**) is depicted in Scheme 2. The desired *β*-KBA based 1*H*-1,2,3-triazole derivatives were achieved by using a three-step synthetic protocol with an amide coupling reaction followed by Jones oxidation and finally a "*click*" reaction. Thereby, in the initial step, the deacetylation of compound **1** (*β*-AKBA) by hydrolysis with 1 M KOH in ^{i}PrOH provided pure **2** (*β*-KBA) in high yield (98%). Step-2 was carried out using amide coupling. In step 2, compound **2** (*β*-KBA) has a free acid group at position C-24 which was reacted with propargyl amine (**3**) in the presence of HATU coupling reagent, to afford the respective *β*-KBA amide (**4**) in high yield (96%). In the next step, compound **4** was oxidized at C-3 position with Jones' reagent (CrO_3/aq. H_2SO_4) in acetone to afford the *β*-KBA keto amide (**5**) in high yield (98%).

The final reaction was carried out by using "*click*" chemistry. In this step, a 1,3-dipolar cycloaddition reaction was conducted between compound **4** and different substituted aromatic azides **6a-6k**, in the presence of copper iodide (CuI) and Hünig's base in MeCN, to obtain the desired products, *β*-KBA skeleton-based 1*H*-1,2,3-triazole derivatives (**7a-7k**) in high yields 90−96%. Under similar conditions, the *β*-KBA keto skeleton-based 1*H*-1,2,3-triazole derivatives (**8a-8k**) were also produced in excellent yields of 92−96% (Table 1).

By analysis of their spectral data (^{1}H- and ^{13}C NMR, HRMS, and ^{19}F-NMR spectroscopy where appropriate), the structures of all new compounds (**4, 5, 7a-7k** and **8a-8k**) were confirmed.

2.1.2. Isolation and Crystal Structure of Compound 4. Compound **4** was obtained as a colorless amorphous powder having a pseudo molecular formula of $C_{33}H_{49}NO_3$ as determined by an *m*/*z* peak at 508.3823 $[M + H]^+$ (calcd. for $C_{33}H_{50}NO_3$, 508.3823) in its HR-ESI-MS (Scheme 1). The ^{1}H NMR spectrum of **4** exhibited two downfield signals at δ_H 3.99−3.90 (2H, m), and 4.05 (1H, m) confirming the presence of one extra methylene and one methine, respectively, which were further confirmed at δ_C 79.6, and 71.6 in the ^{13}C NMR spectrum. Another prominent peak at δ_C 176.2 from δ_C 180.1 further clarified the conversion of the carboxylic acid to amide group. Furthermore, compound **4** crystals were generated from progressive solvent slow evaporation of MeOH at ambient temperature. The detailed stereochemistry of compound **4** was determined by X-ray crystallography (Figure 3).

3. BIOLOGICAL ACTIVITY

The general structural features of the new 24 synthesized alicyclic triterpene amide containing 1*H*-1,2,3-triazole deriva-

https://doi.org/10.1021/acsomega.5c01259
ACS Omega 2025, 10, 21715−21730

Scheme 2. Reagents and Conditions[a]

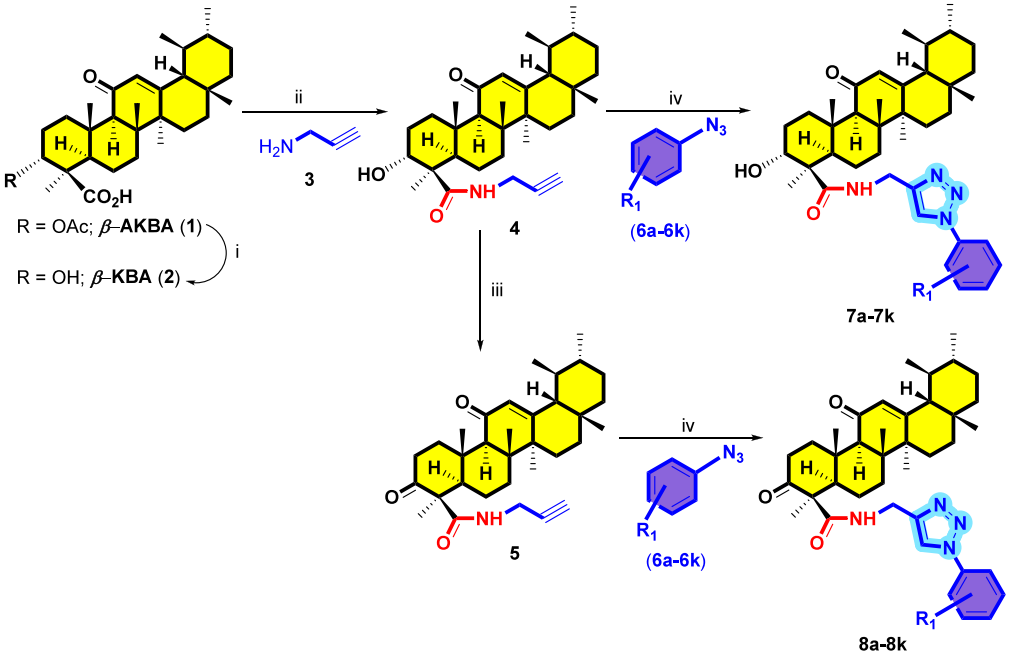

[a](i) 1 N KOH in ^{i}ProH, reflux at 80−85 °C, 6 h, 98%; (ii) propargyl amine (**3**), dry DMF, DIPEA, coupling reagent HATU, room temperature, 18 h, **4** (96%); (iii) Jones' reagent (CrO_3/aq. H_2SO_4), acetone, oxidation at 0 °C to rt, 2 h, **5** (98%); (iv) different substituted aromatic azides (**6a−6k**), Et_3N, CuI, CH_3CN, room temperature, 3 h, **7a−7k** (90-96%) and **8a−8k** (92-96%).

Table 1. Synthesis of Alicyclic Amide Containing 1*H*-1,2,3-triazole Derivatives (7a-7k and 8a-8k)

Reactant	R_1-Group	β-KBA skeleton based 1*H*-1,2,3-triazole derivatives (7a−7k and 8a−8k)	Yields of products 7a-7k and 8a-8k (%)[a]
4	H	7a	92
4	2-F_3C	7b	94
4	2-Me	7c	96
4	2-MeO	7d	92
4	4-Br	7e	90
4	3-Br	7f	92
4	4-MeO	7g	94
4	3-F_3C	7h	92
4	4-F_3C	7i	90
4	4-F	7j	92
4	4-Cl	7k	90
5	H	8a	92
5	2-F_3C	8b	93
5	2-Me	8c	96
5	2-MeO	8d	94
5	4-Br	8e	92
5	3-Br	8f	93
5	4-MeO	8g	96
5	3-F_3C	8h	92
5	4-F_3C	8i	94
5	4-F	8j	93
5	4-Cl	8k	92

[a]Yields refer to pure isolated target products.

tives (**4**, **5**, **7a-7k** and **8a-8k**) are represented in Figure 4. Three variable moieties (β-KBA-skeleton triterpene rigid moiety,

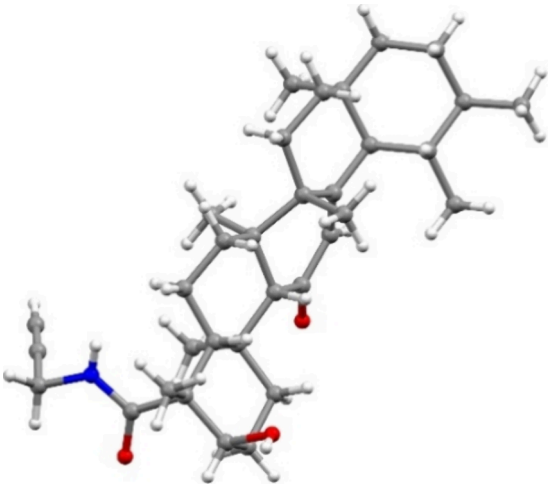

Figure 3. Crystal structure of compound **4**.

alicyclic amide bond, and 1*H*-1,2,3-triazole) were considered as rigid motifs with a β-KBA-skeleton core group attached to the 1*H*-1,2,3-triazole moiety which mainly determined the varied degree of biological activity.

3.1. Anti-proliferative Effects of Compounds. The antiproliferative activities of compounds were evaluated against two human breast cancer cell lines (MDA-MB-231 and MCF-7) and normal HDF cells. Table 2 provides a summary of the effects, with IC_{50} values ranging from 445 μM to 61 μM. Among the compounds, eight derivatives (**7b-7i**) exhibited greater antiproliferative activities than the β-KBA reference compound. In contrast, compounds **8a** through to **8k** showed relatively lower antiproliferative effects compared to β-KBA parent compound. Compound **7f** demonstrated the strongest anti-proliferative effect among all tested compounds, showing

https://doi.org/10.1021/acsomega.5c01259
ACS Omega 2025, 10, 21715−21730

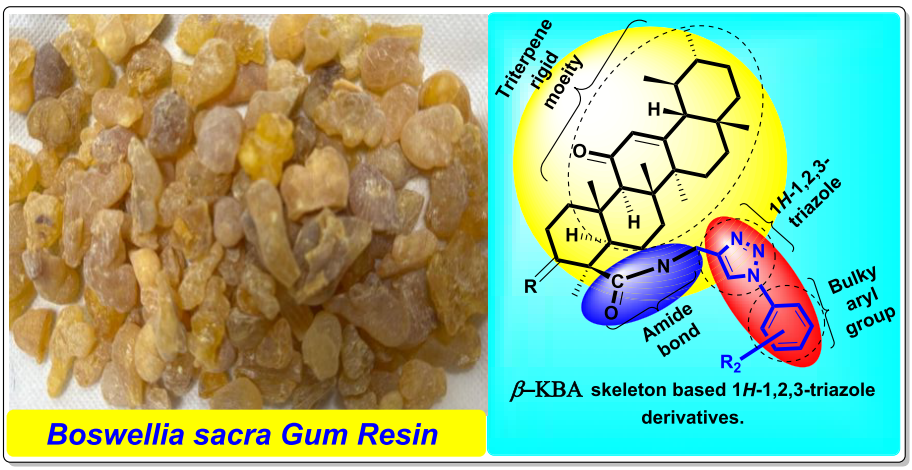

Figure 4. General structural feature of the synthesized alicyclic triterpene amide containing 1*H*-1,2,3-triazole derivatives.

Table 2. Anti-proliferative Effects of β-KBA Derivatives in Human Breast Cancer Cell Lines (MDA-MB-231 and MCF-7), and Normal Human Dermal Cells (HDF)

Compounds	MDA-MB-231 $IC_{50}(\mu M) \pm SEM$	MCF-7 $IC_{50}(\mu M) \pm SEM$	HDF (Normal cell) $IC_{50}(\mu M) \pm SEM$
β-KBA	101.35 ± 3.90	121.61 ± 4.72	194.39 ± 6.01
4	98.43 ± 4.43	111.00 ± 4.72	181.71 ± 7.29
5	115.09 ± 5.91	128.36 ± 6.18	202.09 ± 5.63
7a	102.86 ± 6.74	124.18 ± 7.15	181.32 ± 7.12
7b	69.94 ± 3.45	83.35 ± 4.75	103.41 ± 5.11
7c	64.08 ± 2.96	69.97 ± 3.18	142.35 ± 4.12
7d	71.16 ± 4.15	73.42 ± 2.92	105.18 ± 5.39
7e	72.46 ± 3.62	75.13 ± 2.18	117.36 ± 6.01
7f	61.47 ± 2.18	67.02 ± 3.12	121.15 ± 4.68
7g	76.61 ± 3.65	78.96 ± 3.01	108.92 ± 5.34
7h	70.42 ± 2.72	73.24 ± 3.19	116.47 ± 3.16
7i	65.34 ± 2.30	80.73 ± 3.48	113.31 ± 5.39
7j	71.43 ± 3.98	76.39 ± 3.16	107.52 ± 6.14
7k	106.26 ± 7.21	134.23 ± 6.32	191.39 ± 8.13
8a	228.59 ± 7.32	245.48 ± 8.21	289.16 ± 9.50
8b	268.43 ± 8.27	273.25 ± 7.36	326.29 ± 9.21
8c	341.72 ± 9.48	386.61 ± 10.17	445.37 ± 10.06
8d	329.19 ± 10.21	367.48 ± 9.16	433.19 ± 12.21
8e	352.31 ± 11.09	371.72 ± 8.36	441.41 ± 8.16
8f	338.81 ± 12.31	374.19 ± 10.56	426.23 ± 7.77
8g	225.08 ± 8.21	249.28 ± 9.67	293.69 ± 9.48
8h	236.41 ± 7.46	253.44 ± 6.39	311.75 ± 8.35
8i	274.79 ± 6.92	299.21 ± 4.26	339.09 ± 9.13
8j	264.92 ± 6.23	291.71 ± 5.93	341.11 ± 10.19
8k	336.36 ± 9.41	351.17 ± 10.81	432.21 ± 11.26

significant activity even at lower concentrations. This potency against HDF cells, as normal cells, led to its selection for further immunoactivity testing on PBMCs at concentrations of 5 μM (IC_{95}) and 10 μM (IC_{90}).

3.2. Modulation of T Cell Subset Populations and Immune Checkpoint Expression. We evaluated the expression of T cell subsets in PBMCs treated with different concentrations of the **7f** derivative of β-KBA. The analysis focused on two primary T cell populations: CD4- CD8+ (cytotoxic T cells) and CD4+ CD8- (helper T cells). Regarding the CD4- CD8+ T cell subset, the average percentages were 37% in the control group, 39% at a 5 μM concentration of **7f**, and 36% at a 10 μM of **7f**. In contrast, the CD4+ CD8- T cell subset showed average percentages of 30% in the control group, 40% at 5 μM, and 40.5% at 10 μM of **7f**. We also assessed the expression of immune checkpoints PD-1 and TIGIT within these T cell subsets. In the CD4- CD8+ T cells, PD-1 expression was measured at 17.6% in the control group, increasing to 22.1% at a 5 μM concentration and slightly decreasing to 20.2% at 10 μM of **7f**. TIGIT expression in this subset was 7.69% in the control group, rising to 9.83% at 5 μM and dropping to 8.36% at 10 μM of **7f**. For the CD4+ CD8- T cell subset, PD-1 expression was 14.1% in the control group, increasing to 16.1% at 5 μM and decreasing to 8.23% at 10 μM of **7f**. The TIGIT expression in this subset was measured at 7.53% in the control group, increasing to 11.6% at 5 μM and subsequently declining to 9.88% at 10 μM of **7f** (Figure 5).

3.3. Molecular Docking Studies. A total of nine compounds (**7b**-**7j**) showed significant inhibitory potential in two human breast cancer cell lines (MDA-MB-231 and MCF-7) compared to the standard molecule. We selected CDK-4 as a potential drug target because of its expression in both MDA-MB-231 and MCF-7 cell lines. Docking analysis of the most active inhibitors with CDK-4 reflects the good binding potential of those molecules toward CDK-4. All molecules were well accommodated in the ligand binding cavity of CDK-4. The most active molecule **7f**, exhibited the highest docking score with excellent interactions with Glu94, Val96, Phe93, Ile12 and Gln98. The molecules mediated both hydrogen bonding and hydrophobic interactions with these residues. The − OH group of KBA moiety and the amide group of **7f** specifically formed hydrogen bonds with the carbonyl oxygen of Glu94 and amino nitrogen of Val96 at 2.04 Å and 2.22 Å, respectively. The side chain of Ile12 and Cα of Gln98 provided hydrophobic interactions to the triazole and bromophenyl rings of this compound. Moreover, the side chain of Phe93 also mediated a hydrophobic interaction with the KBA moiety of **7f**.

Due to these interactions, compound **7f** exhibited a higher docking score, i.e. − 7.70 kcal/mol. The second most active compound **7c** showed interactions with Tyr17 and Leu147. The carbonyl moiety of KBA and the triazole ring of this compound formed a hydrogen bond and a hydrophobic interaction with the side chain − OH of Tyr17 (1.74 Å) and side chain of Leu147 (3.20 Å), respectively. The conformation of **7c** was similar to that of **7f**, however, the − OH, amide and the toluene groups of **7c** did not interact with the surrounding residues. Due to this

https://doi.org/10.1021/acsomega.5c01259
ACS Omega 2025, 10, 21715−21730

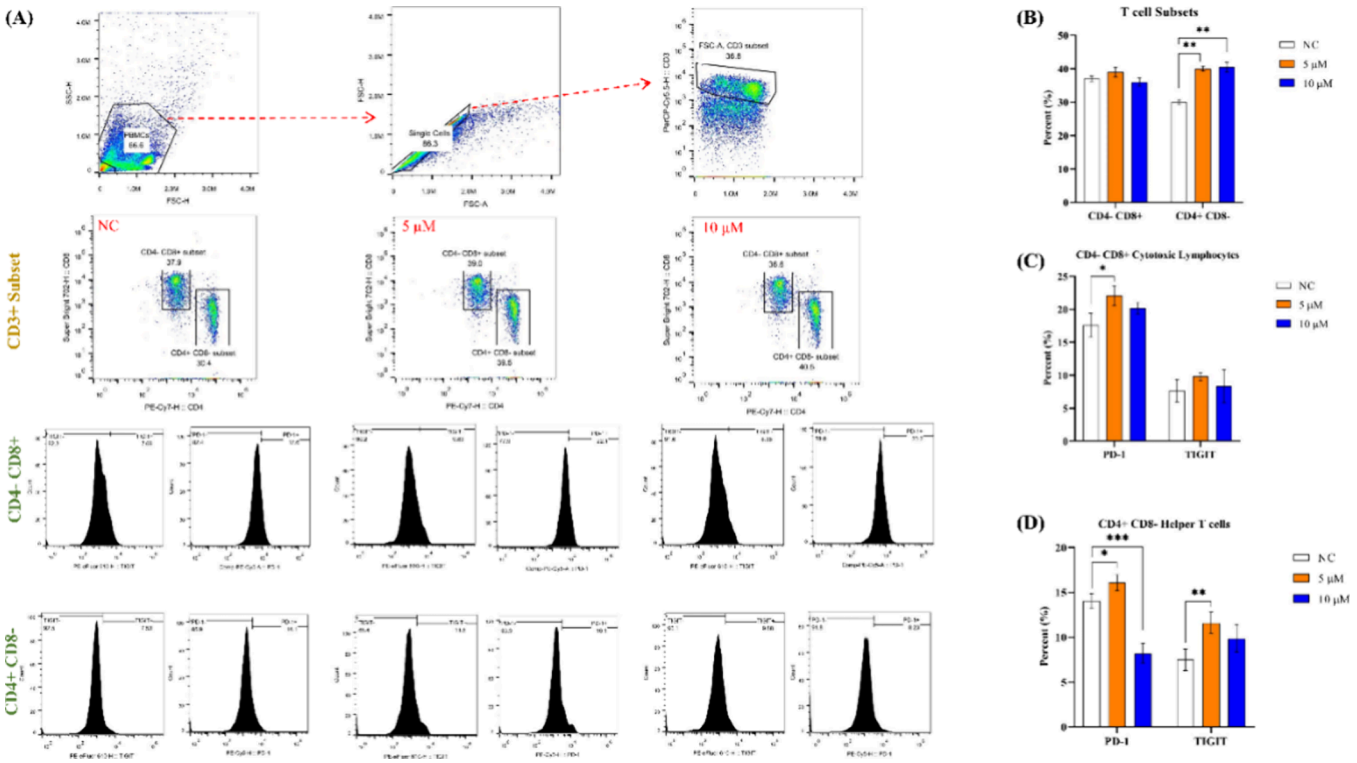

Figure 5. Analysis of T cell subset frequencies and immune checkpoint expression in PBMCs treated with varying concentrations of the **7f** derivative of *β*-KBA. PBMCs were treated with the **7f** derivative of KBA at concentrations of 5 μM and 10 μM, with untreated cells serving as the control (NC). (A) The gating strategy used to identify CD4+ CD8- (helper T cells) and CD4- CD8+ (cytotoxic T cells) populations are shown. (B) The average percentage of each subset in the control, 5 μM, and 10 μM conditions. (C) PD-1 and TIGIT expression on CD4- CD8+ T cells. (D) PD-1 and TIGIT expression on CD4+ CD8- T cells. Each bar represents the mean ± standard deviation (SD) of three replicates from each donor, with total replicates (n = 18) across all six donors. Fluorescence minus one (FMO) and isotype controls were used to define positive populations. An asterisk (*) indicates statistical significance (*p < 0.05; **p < 0.01; ***p < 0.001) compared to the control (NC), as calculated using appropriate statistical tests.

reason, **7c** exhibited a slightly lower docking score (−7.66) than **7f**. After **7f** and **7c**, compounds **7i** and **7b** showed significant antiproliferative potential. In contrast to **7c**, **7i** interacted with the amide nitrogen of Val14 and side chain of Lys142 through its − OH and amide groups at 1.98 Å and 1.92 Å, respectively. Moreover, the side chains of Val20 and Phe93 mediated hydrophobic interactions with the triazole and the trifluoromethyl phenyl rings, respectively. Interestingly, the polar moieties of **7b**, including carbonyl and hydroxyl oxygens of KBA and the amide nitrogen, formed hydrogen bonds with the side chain − OH of Tyr17 (1.92 Å), the amide oxygen of Ile12 (2.22 Å) and the amide oxygen of Glu144 (2.17 Å). Both **7i** (−7.64 kcal/mol) and **7b** (−7.58 kcal/mol) exhibited docking scores comparable to that of **7c**.

Compounds **7h**, **7d**, **7j**, **7e** and **7g** demonstrated IC_{50} values in the range of 70 to >78 μM and these molecules were also considered as good inhibitors. Interestingly, the triazole nitrogen of **7h** mediated bidentate interactions with Lys22 (2.05 Å and 2.16 Å) and a hydrophobic interaction with Asp97, while the amide nitrogen of **7h** formed a hydrogen bond with the carbonyl oxygen of Val96 at 2.07 Å. Furthermore, the side chain of Phe93 formed a hydrophobic interaction with the KBA scaffold of **7h**. The binding mode of **7d** showed its interactions with Glu94 and Gln98. The − OH and anisole ring of **7d** formed a hydrogen bond with the amide oxygen of Glu94 at 2.10 Å, and a hydrophobic interaction with Gln98 (3.84 Å), respectively. Likewise, the − OH of **7j** also formed a hydrogen bond with the amide oxygen of Glu94 (1.99 Å), whereas the amide oxygen of this molecule interacted with the amino group of Val96 via a hydrogen bond (2.08 Å). Moreover, the triazole moiety of **7j** was stabilized through hydrophobic interactions with Ile12 and Lys22. The − OH of **7e** formed a hydrogen bond with the amino group of Val96 at 2.11 Å, while Phe93 and Ile12 mediated multiple hydrophobic interactions with the KBA and the triazole groups of **7e**. Unlike the rest of the docked molecules, compound **7g** was only stabilized through a hydrophobic interaction with Phe93 at the ligand binding site. Compounds (**7h**, **7d**, **7j**, **7e**, and **7g**) exhibited docking scores in range of −7.38 to − 7.12 kcal/mol. The docking scores of the docked complexes aligned well with the inhibitory potential of these molecules. The docking results are given in Table 3 and the binding modes of the compounds are shown in Figure 6.

The evaluation of the antiproliferative activities of synthesized compounds against two human breast cancer cell lines, and normal HDF cells revealed that eight derivatives (**7b**−**7i**) exhibited appreciable antiproliferative effects compared to the *β*-KBA reference compound. Compound **7f** emerged as the most potent, demonstrating strong antiproliferative effects at lower concentrations. This potency is especially advantageous in drug development, as effective low doses can potentially minimize toxicity and reduce side effects.[39]

To better understand the immunomodulatory potential of compound **7f**, we examined its effects on T cell subsets and the expression of immune checkpoints, PD-1 and TIGIT, in CD4- CD8+ (cytotoxic T cells) and CD4+ CD8- (helper T cells) populations. The **7f** derivative of *β*-KBA showed no substantial impact on the overall proportion of CD4- CD8+ T cells, and remained unchanged across treatment conditions, while CD4+

https://doi.org/10.1021/acsomega.5c01259
ACS Omega 2025, 10, 21715−21730

Table 3. Molecular Docking Results of Most Active Compound with CDK-4[a]

Compounds	Score (kcal/mol)	Ligand	Receptor	Interaction	Distance (Å)
7b	−7.58	N71	O-GLU144	HBD	2.17
		O83	O-ILE12	HBD	2.22
		O70	OH-TYR17	HBA	1.92
7c	−7.66	O70	OH-TYR17	HBA	1.74
		5-ring	CD2-LEU147	π-H	3.20
7d	−7.27	O83	O-GLU94	HBD	2.10
		6-ring	CA-GLN98	π-H	3.84
7e	−7.15	O73	N-VAL96	HBA	2.11
		C47	6-ring-PHE93	H-π	3.49
		O83	6-ring-PHE93	H-π	3.17
		5-ring	CG2-ILE12	π-H	4.32
7f	−7.70	O81	O-Glu94	HBD	2.04
		O71	N-Val96	HBA	2.22
		C45	6-ring-Phe93	H-π	3.69
		5-ring	CG2-Ile12	π-H	4.18
		6-ring	CA-Gln98	π-H	4.17
7g	−7.12	C47	6-ring-PHE93	H-π	2.81
7h	−7.38	N71	O-VAL96	HBD	2.07
		N78	NZ-LYS22	HBA	2.05
		N82	NZ-LYS22	HBA	2.16
		C47	6-ring-PHE93	H-π	2.61
		5-ring	CA-ASP97	π-H	4.13
7i	−7.64	O73	NZ-LYS142	HBA	1.92
		O83	N-VAL14	HBA	1.98
		C88	6-ring-PHE93	H-π	3.40
		5-ring	CG2-VAL20	π-H	3.83
7j	−7.24	O83	O-GLU94	HBD	1.99
		O73	N-VAL96	HBA	2.08
		5-ring	CG2-ILE12	π-H	4.50
		5-ring	NZ-LYS22	π-cation	2.66

[a]HBA = Hydrogen bond acceptor, HBD = Hydrogen bond donor.

CD8- T cell frequencies slightly increased at both 5 μM and 10 μM concentrations. These findings indicated that **7f** selectively impacts helper T cells, possibly through mechanisms influencing cell proliferation and survival that are more active in CD4+ T cells, which may eventually enhance T cell activation and function.[40]

In CD4- CD8+ T cells, PD-1 expression increased upon treatment, peaking at 5 μM before a slight decline at 10 μM. Similarly, TIGIT expression was elevated at 5 μM but decreased at higher concentration. This biphasic response in immune checkpoint expression suggests that a low dose of **7f** enhances T cell inhibitory pathways, probably as a compensatory mechanism to control overactivation.[41] Elevated PD-1 and TIGIT at 5 μM could point toward an increase in the immune suppression profile of cytotoxic T cells, indicating that the **7f** at low doses may temper T cell cytotoxic activity, which can be desirable in inflammatory settings where excessive cytotoxicity could lead to tissue damage.[42] The reduction in PD-1 and TIGIT expression at 10 μM might reflect saturation effects or an inhibitory feedback mechanism where higher concentrations counterbalance the initial immune-modulating effect.

In CD4+, CD8- T cells, PD-1 expression increased slightly at 5 μM but decreased significantly at 10 μM, and TIGIT expression followed a similar pattern. This decrease at higher concentrations may be due to differential sensitivity of helper T cells to **7f** derivative treatment, suggesting that these cells may resist prolonged inhibitory signaling under conditions of higher compound exposure.[43] The reduced PD-1 and TIGIT expression observed at a 10 μM concentration suggests that the **7f** derivative, at higher doses, may interfere with the typical checkpoint regulation in helper T cells. This disruption leads to lower levels of inhibitory receptor expression, which could favor T cell activation. Such a trend indicates that the **7f** derivative may enhance helper T cell activity by decreasing inhibitory signaling at elevated doses.[44]

Docking plays an important role in the determination of binding potential of a drug-like molecule with its potential target in the physiological system, which ultimately helps in the acceleration of drug discovery process.[34,45] We have determined the binding mode of some of the most active antiproliferative agents identified in this study using molecular docking strategy. For docking, CDK-4 was selected as the potential drug target because of its expression in triple-negative breast cancer (MDA-MB-231) and estrogen receptor-positive (MCF-7) breast cancer cell lines. CDK4 is a key regulator of the cell cycle and is involved in the transition from the G1 phase to the S phase, where cell proliferation is initiated. Overexpression or dysregulation of CDK4 is observed in various cancers, including breast cancer, as it can drive uncontrolled cell division and contribute to tumorigenesis.[46−50,51−54] When docked at the ligand binding site where a molecule of abemaciclib is cocrystallized in the X-ray structure of CDK-4, our compounds showed excellent binding interactions, and highly negative docking scores, reflecting their good binding potential for CDK-4. All ligands completely blocked the ligand binding site of CDK-4. We observed a good role of Glu94 and Val96 in the stabilization of our compounds at the ligand binding site through hydrogen bonds, whereas Phe93 mainly provided hydrophobic interactions to these molecules. The − OH at KBA moiety, the amide linker and the triazole nitrogen are the key pharmacophores which mediate hydrophilic interactions with the surrounding residues, while KBA and the R group forms hydrophobic interactions at the ligand binding site. This indicates that further modification of functional moieties can lead to the formation of more potent antiproliferative molecules.

4. CONCLUSIONS

Currently, we have reported the synthesis of 24 undescribed alicyclic triterpene-amide (**4**, **5**, **7a−7k** and **8a−8k**) containing 1*H*-1,2,3-triazole derivatives. All newly synthesized compounds were confirmed by advanced spectroscopic techniques via., ^{1}H-, ^{13}C-, ^{19}F-NMR (where is applicable), and HR-ESI-MS. The stereochemistry of compound **4** was confirmed by X-ray crystallography. The antibreast cancer activity of the prepared compounds was screened using human breast cancer cell lines. Among the synthetic compounds, eight derivatives (**7b-7i**) exhibited notable antiproliferative activities compared to β-KBA (**2**). Similarly, compound **7f** displayed a remarkable effect

https://doi.org/10.1021/acsomega.5c01259
ACS Omega 2025, 10, 21715−21730

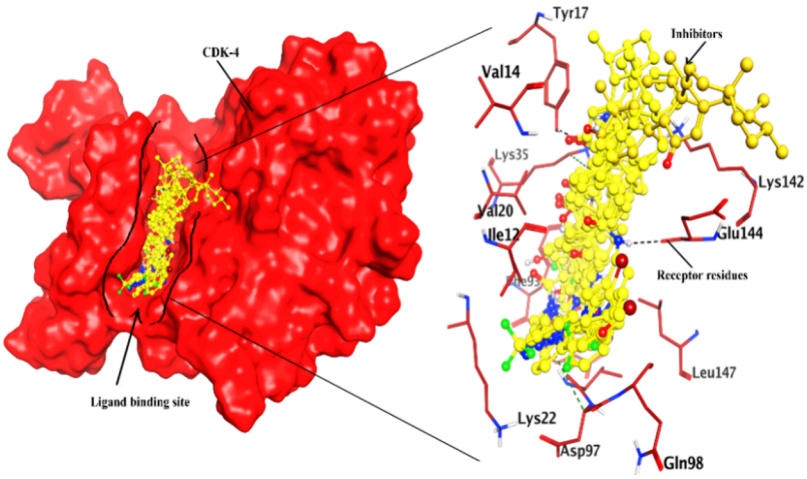

Figure 6. Binding modes of compounds are shown in the binding cavity of CDK-4. Compounds are depicted in yellow ball and stick model, interacting residues and protein are shown in red color, while hydrogen bonds and hydrophobic interactions are displayed in black and green dashed lines, respectively.

among all screened compounds, representing significant activity even at lower concentrations. Furthermore, compound **7f** significantly expanded CD4+ CD8- helper T cell population at both 5 μM and 10 μM concentrations, increasing the expression of PD-1 and TIGIT immune checkpoints at 5 μM. The binding capacity of the most active compounds were exhibited through in-silico docking studies by CDK4 (cyclin-dependent kinase 4) as a prominent target. The binding interactions and docking scores of compounds at the CDK-4 ligand binding site might possibly be due to the − OH at the C-3 position of KBA, the amide-linkage and 1*H*-1,2,3-triazole moiety in the binding site of synthesized compounds.

5. EXPERIMENTAL SECTION

5.1. General. All reagents were obtained from Sigma-Aldrich, Germany. Silica gel for column chromatography was 100−200 mesh. Solvents were purified by following standard procedures. High-resolution electrospray ionization mass spectra (HR-ESI-MS) were recorded on an Agilent 6530 LC Q-TOF instrument. The ^{1}H- and ^{13}C NMR spectra were recorded on a Bruker NMR spectrometer (600 MHz for ^{1}H, 150 MHz for ^{13}C and 564 MHz for ^{19}F) using $CDCl_3$ as a solvent. Thin layer chromatography (TLC) was carried using silica gel F_{254} precoated plates. UV-light and I_2 stain were used to visualize the spots. Organic extracts and solutions of pure compounds were dried over anhydrous $MgSO_4$. Crystal data are summarized in Table S1. A single crystal of compound **4** was mounted on a MiTeGen loop with grease and examined on a Bruker D8 Venture APEX diffractometer equipped with a Photon 100 CCD area detector at 296 (2) K using graphite monochromatized Mo−K_α radiation (λ = 0.71073Å). Data were collected using the APEX 4 software,[1] integrated using SAINT,[2] and corrected for absorption using a multiscan approach (SADABS).[3] Final cell constants were determined from full least-squares refinement of all observed reflections. The structure was solved using intrinsic phasing (SHELXT).[4] All non-H atoms were in subsequent difference maps and refined anisotropically. H atoms were added at calculated positions and refined with a riding model. The structure of compound **4** has been deposited with the **CCDC** (CCDC deposition number = **2419825**).

5.2. Synthesis of N-(Prop-2-yne-1-yl)-3α-hydroxy-11-oxours-12-en-24-carboxamide (4). To a solution of β-KBA (**2**) (1.0 equiv) in dry DMF (10 mL) were added successively propargylamine **3** (1.1 equiv), HATU coupling agent (1.2 equiv) and *N*,*N*-diisopropylethylamine (DIPEA) (2.5 equiv) as a base. The reaction mixture was stirred at room temperature for 18 h until completion of the reaction (monitored by TLC analysis). After completion of the reaction, it was extracted with EtOAc (3 × 30 mL). The crude product was obtained by drying the combined organic layer over anhydrous $MgSO_4$ and then concentrating it under reduced pressure on a rotary evaporator. The crude product was then purified using column chromatography on silica gel with *n*-hexane/ethyl acetate (85:15 v/v) as an eluent to yield pure compound **4** (96%); Dark brown solid, crystals developed in MeOH; Yield = 96%; mp 218−220 °C; ^{1}H NMR (600 MHz, $CDCl_3$) δ 5.70 (t, J = 5.3 Hz, 1H), 5.56 (d, J = 5.0 Hz, 1H), 4.13 (d, J = 2.8 Hz, 1H), 4.05 (ddd, J = 24.7, 5.1, 2.5 Hz, 2H), 3.06 (s, 1H), 2.81 (s, 1H), 2.52 (d, J = 3.4 Hz, 1H), 2.45 (s, 1H), 2.40 (s, 1H), 2.24 (t, J = 2.5 Hz, 1H), 2.10 (d, J = 4.8 Hz, 2H), 1.89 (td, J = 13.7, 5.1 Hz, 2H), 1.80 − 1.73 (m, 3H), 1.60 − 1.51 (m, 5H), 1.48 (q, J = 3.8 Hz, 2H), 1.45 (d, J = 6.5 Hz, 2H), 1.33 (s, 3H), 1.28 (s, 3H), 1.21 (s, 3H), 1.13 (s, 3H), 1.04 − 1.01 (m, 1H), 0.95 (s, 3H), 0.83 (s, 3H), 0.80 (d, J = 6.5 Hz, 3H); ^{13}C NMR (150 MHz, $CDCl_3$) δ 199.3, 176.2, 164.9, 130.5, 79.5, 71.5, 70.6, 60.4, 59.0, 55.6, 48.7, 47.3, 45.0, 43.8, 40.9, 39.3, 38.6, 37.5, 34.1, 34.0, 33.1, 30.9, 29.1, 28.8, 27.5, 27.1, 26.5, 24.9, 21.1, 20.5, 19.5, 18.3, 17.4, 13.3; ^{13}C DEPT90 NMR (150 MHz, $CDCl_3$) δ 130.5, 79.5, 70.6, 60.4, 59.0, 55.6, 48.7, 39.3; ^{13}C DEPT135 NMR (150 MHz, $CDCl_3$) δ 130.5, 70.6, 60.4, 59.0, 48.7, 40.9, 39.3, 34.1, 33.1, 30.9, 29.1, 28.8, 26.5, 24.9, 21.1, 20.5, 19.5, 18.3, 17.4, 13.3; HRMS (ESI$^+$) calcd. for $C_{33}H_{50}NO_3$ $[M + H]^+$ 508.3525, found 508.3823. Elemental analysis: $C_{33}H_{49}NO_3$ calcd.: C, 78.08; H, 9.75; N, 2.78; O, 9.45; found: C, 78.06; H, 9.73; N, 2.76; O, 9.45.

5.3. Synthesis of N-(Prop-2-yne-1-yl)-3,11-dioxours-12-en-24-carboxamide (5). A stirred solution of compound **4** (1.0 equiv) suspended in 10 mL acetone received dropwise addition of Jones reagent (1.0 mL) at 0 °C and stirred at room temperature for 2 h. Upon completion, as determined by TLC, the reaction was quenched with water at 0 °C and ^{i}PrOH was added, and the reaction mixture was stirred for 30 min. After completion of the reaction, it was extracted with CH_2Cl_2 (3 × 30 mL). The crude product was obtained by drying the combined organic layer over anhydrous Na_2SO_4 and then concentrating it

https://doi.org/10.1021/acsomega.5c01259
ACS Omega 2025, 10, 21715−21730

under reduced pressure on a rotary evaporator. The crude product was then purified using column chromatography on silica gel with *n*-hexane/ethyl acetate (85:15 v/v) as an eluent to yield pure compound **5** in a high yield (98%); White solid; Yield = 98%; mp 212−214 °C; ^{1}H NMR (600 MHz, $CDCl_3$) δ 5.78 (t, J = 5.3 Hz, 1H), 5.57 (s, 1H), 3.96 (dd, J = 5.3, 2.5 Hz, 2H), 3.06 − 2.94 (m, 2H), 2.42 − 2.37 (m, 2H), 2.26 − 2.20 (m, 2H), 2.12 − 1.99 (m, 4H), 1.93 − 1.88 (m, 1H), 1.83 − 1.79 (m, 1H), 1.65 − 1.61 (m, 1H), 1.57 − 1.44 (m, 5H), 1.39 (s, 3H), 1.37 (s, 3H), 1.35 − 1.31 (m, 2H), 1.28 (s, 3H), 1.24 (s, 3H), 1.22 − 1.19 (m, 1H), 1.04 − 1.00 (m, 1H), 0.94 (s, 3H), 0.83 (s, 3H), 0.79 (d, J = 6.4 Hz, 3H); ^{13}C NMR (150 MHz, $CDCl_3$) δ 211.8, 198.7, 172.1, 165.4, 130.3, 79.1, 71.6, 60.1, 59.0, 58.7, 58.1, 44.8, 43.7, 40.8, 39.2, 37.1, 33.9, 33.0, 30.8, 29.2, 28.8, 27.4, 27.3, 22.3, 21.1, 20.3, 20.2, 18.3, 17.4, 14.1; ^{13}C DEPT135 NMR (150 MHz, $CDCl_3$) δ 130.3, 60.1, 59.0, 58.1, 40.8, 39.2, 37.1, 33.0, 30.8, 29.2, 28.8, 27.4, 27.2, 22.3, 21.1, 20.3, 20.2, 18.3, 17.4, 14.1; ^{13}C DEPT90 NMR (150 MHz, $CDCl_3$) δ 130.3, 71.6, 60.1, 59.0, 58.1, 39.2; HRMS (ESI$^+$) calcd. for $C_{33}H_{48}NO_3$ $[M + H]^+$ 506.4990 found 506.4993. Elemental analysis: $C_{33}H_{47}NO_3$ calcd.: C, 78.39; H, 9.35; N, 2.78; O, 9.51; found: C, 78.37; H, 9.37; N, 2.77; O, 9.49.

5.4. General Procedure for Synthesis of *β*-KBA Skeleton Based 1*H*-1,2,3-triazole Derivatives. CuI (2.0 equiv) and Et_3N (3.0 equiv) were added to a solution of compound **4** or compound **5** (1.0 equiv) and substituted aromatic azides **6a**−**6k** (1.2 equiv) in acetonitrile (10 mL), and the mixture was stirred for 3 h (3 h). The mixture was then stirred at room temperature for 3 h until the reaction was complete (as reported by TLC analysis). After completion of the reaction, the reaction mixture was diluted with EtOAc (30 mL), 15 mL of aqueous saturated NH_4Cl solution was added, and the aqueous layer was extracted with EtOAc (3 × 30 mL). Then, the combined organic layer was washed with brine (1 × 20 mL), dried over anhydrous $MgSO_4$, filtered, and the filtrate was concentrated in vacuo. The crude residue was further purified by flash column chromatography (silica gel, *n*-hexane/EtOAc, 75:25) to furnish the desired pure *β*-KBA skeleton based 1*H*-1,2,3-triazole derivatives **7a**−**7k** (90−96%) and **8a**−**8k** (92−96%).

*5.4.1. N-((1-Phenyl-1H-1,2,3-triazol-4-yl)methyl)-3α-hydroxy-11-oxours-12-en-24-carboxamide (**7a**).* Gummy dark yellow solid; Yield = 92%; ^{1}H NMR (600 MHz, $CDCl_3$) δ 8.02 (s, 1H), 7.71 (d, J = 7.9 Hz, 2H), 7.55 (d, J = 7.8 Hz, 2H), 7.47 (d, J = 7.4 Hz, 1H), 7.38 (d, J = 7.8 Hz, 1H), 7.05 (d, J = 7.9 Hz, 1H), 6.41 (d, J = 6.0 Hz, 1H), 5.53 (s, 1H), 4.69 − 4.57 (m, 2H), 4.14 (t, J = 5.2 Hz, 2H), 2.93 (d, J = 7.4 Hz, 3H), 2.82 (s, 3H), 2.48 (d, J = 17.2 Hz, 3H), 2.10 (s, 1H), 2.06 (s, 2H), 1.88 (d, J = 5.1 Hz, 1H), 1.80 (d, J = 8.8 Hz, 2H), 1.73 (t, J = 10.2 Hz, 1H), 1.61 − 1.57 (m, 1H), 1.53 (d, J = 10.7 Hz, 3H), 1.47 (s, 1H), 1.32 (s, 3H), 1.29 (d, J = 8.2 Hz, 3H), 1.15 (s, 3H), 1.03 (dd, J = 9.7, 5.3 Hz, 1H), 0.95 (s, 3H), 0.82 (s, 3H), 0.80 (d, J = 6.6 Hz, 3H); ^{13}C NMR (150 MHz, $CDCl_3$) δ 199.3, 176.7, 164.9, 145.1, 136.9, 130.5, 129.8, 128.9, 124.8, 119.0, 70.7, 60.4, 59.0, 48.7, 47.3, 46.3, 45.0, 43.8, 40.9, 39.2, 38.6, 37.5, 34.7, 34.1, 33.9, 33.1, 30.9, 28.8, 27.5, 27.1, 26.5, 25.0, 21.1, 20.5, 19.6, 18.2, 17.4, 14.2, 13.0; HRMS (ESI$^+$) calcd. for $C_{39}H_{55}N_4O_3$ $[M + H]^+$ 627.4183 found 627.4181. Elemental analysis: $C_{39}H_{54}N_4O_3$ calcd.: C, 74.75; H, 8.66; N, 8.92; O, 7.68; found: C, 74.72; H, 8.68; N, 8.94; O, 7.66.

*5.4.2. N-((1-(2-(trifluoromethyl)phenyl)-1H-1,2,3-triazol-4-yl)methyl)-3α-hydroxy-11-oxours-12-en-24-carboxamide (**7b**).* Red brown solid; Yield = 94%; ^{1}H NMR (600 MHz, $CDCl_3$) δ 7.89 − 7.85 (m, 2H), 7.75 (td, J = 7.7, 1.6 Hz, 1H), 7.70 (t, J = 7.7 Hz, 1H), 7.62 (dd, J = 21.1, 1.5 Hz, 1H), 7.49 (d, J = 7.8 Hz, 1H), 6.45 (t, J = 5.8 Hz, 1H), 5.53 (s, 1H), 4.70 − 4.55 (m, 2H), 4.14 (d, J = 3.0 Hz, 1H), 2.91 (q, J = 7.4 Hz, 3H), 2.81 (s, 2H), 2.43 (s, 1H), 2.11 − 2.04 (m, 2H), 1.90 − 1.85 (m, 1H), 1.80 (q, J = 6.2 Hz, 2H), 1.73 (dd, J = 12.6, 7.0 Hz, 1H), 1.59 − 1.54 (m, 2H), 1.50 (ddt, J = 12.3, 9.4, 4.5 Hz, 4H), 1.47 − 1.44 (m, 1H), 1.31 (s, 3H), 1.28 (s, 3H), 1.26 (d, J = 3.8 Hz, 3H), 1.23 − 1.20 (m, 1H), 1.15 (s, 3H), 1.03 − 1.00 (m, 1H), 0.95 (s, 3H), 0.81 (s, 3H), 0.79 (d, J = 6.4 Hz, 3H); ^{13}C NMR (150 MHz, $CDCl_3$) δ 199.3, 176.7, 164.9, 144.5, 134.6, 133.1, 130.5, 128.9, 124.4, 119.5, 117.1, 70.6, 60.4, 59.0, 48.7, 47.3, 46.3, 45.0, 43.8, 40.9, 39.2, 38.6, 37.5, 34.5, 34.1, 33.9, 33.1, 30.9, 28.8, 27.4, 27.1, 26.5, 25.0, 21.1, 20.5, 19.6, 18.2, 17.4, 13.1; ^{19}F NMR (565 MHz, $CDCl_3$) δ − 58.8; HRMS (ESI$^+$) calcd. for $C_{40}H_{54}F_3N_4O_3$ $[M + H]^+$ 695.6646 found 695.6648. Elemental analysis: $C_{40}H_{53}F_3N_4O_3$ calcd.: C, 69.16; H, 7.67; F, 8.23; N, 8.08; O, 6.91; found: C, 69.14; H, 7.69; F, 8.20; N, 8.06; O, 6.91.

*5.4.3. N-((1-(o-tolyl)-1H-1,2,3-triazol-4-yl)methyl)-3α-hydroxy-11-oxours-12-en-24-carboxamide (**7c**).* Gummy brown solid; Yield = 96%; ^{1}H NMR (600 MHz, $CDCl_3$) δ 7.78 (s, 1H), 7.42 (d, J = 7.9 Hz, 1H), 7.24 (s, 1H), 7.17 (d, J = 7.5 Hz, 1H), 7.13 (d, J = 7.8 Hz, 1H), 7.05 (d, J = 7.6 Hz, 1H), 6.53 (s, 1H), 5.53 (s, 1H), 4.71 (dd, J = 15.1, 6.0 Hz, 1H), 4.56 (dd, J = 14.9, 5.3 Hz, 1H), 4.14 (t, J = 5.2 Hz, 2H), 2.85 (s, 3H), 2.84 (s, 3H), 2.46 (d, J = 14.8 Hz, 2H), 2.22 (s, 3H), 2.11 − 2.08 (m, 1H), 2.06 (d, J = 1.4 Hz, 2H), 2.02 (d, J = 1.4 Hz, 3H), 1.87 (d, J = 5.1 Hz, 1H), 1.83 − 1.80 (m, 2H), 1.71 (d, J = 8.4 Hz, 1H), 1.51 (d, J = 12.7 Hz, 3H), 1.46 (s, 1H), 1.31 (s, 3H), 1.29 (s, 3H), 1.13 (s, 3H), 1.03 (s, 1H), 0.92 (s, 3H), 0.81 (s, 3H), 0.80 (s, 3H); ^{13}C NMR (150 MHz, $CDCl_3$) δ 199.3, 176.7, 164.9, 144.3, 136.2, 133.6, 131.5, 131.1, 127.0, 125.9, 124.5, 117.8, 70.6, 60.4, 59.0, 48.7, 47.3, 46.3, 45.0, 43.8, 40.9, 39.2, 38.6, 37.5, 33.9, 33.0, 30.9, 28.8, 27.4, 25.1, 21.1, 20.5, 19.7, 18.2, 17.8, 17.4, 13.2; HRMS (ESI$^+$) calcd. for $C_{40}H_{57}N_4O_3$ $[M + H]^+$ 641.3182 found 641.3180. Elemental analysis: $C_{40}H_{56}N_4O_3$ calcd.: C, 74.98; H, 8.83; N, 8.72; O, 7.47; found: C, 74.96; H, 8.81; N, 8.74; O, 7.49.

*5.4.4. N-((1-(2-methoxyphenyl)-1H-1,2,3-triazol-4-yl)methyl)-3α-hydroxy-11-oxours-24-carboxamide (**7d**).* Gummy red solid; Yield = 92%; ^{1}H NMR (600 MHz, $CDCl_3$) δ 8.13 (s, 1H), 7.71 − 7.66 (m, 1H), 7.43 (td, J = 7.9, 1.7 Hz, 1H), 7.02 (dd, J = 7.9, 1.7 Hz, 1H), 6.95 (dd, J = 7.6, 1.3 Hz, 1H), 6.90 (dd, J = 8.2, 1.3 Hz, 1H), 6.58 (t, J = 5.8 Hz, 1H), 5.51 (s, 1H), 4.69 (d, J = 9.2 Hz, 1H), 4.60 (dd, J = 14.9, 5.4 Hz, 1H), 4.16 − 4.10 (m, 2H), 3.88 (s, 3H), 2.92 (d, J = 7.3 Hz, 3H), 2.81 (s, 3H), 2.48 − 2.34 (m, 4H), 2.08 (d, J = 4.8 Hz, 1H), 1.90 − 1.80 (m, 4H), 1.74 − 1.65 (m, 2H), 1.54 (d, J = 3.4 Hz, 1H), 1.49 (d, J = 12.2 Hz, 3H), 1.45 − 1.42 (m, 1H), 1.30 (s, 3H), 1.28 (s, 3H), 1.25 (s, 3H), 1.21 − 1.18 (m, 1H), 1.12 (s, 3H), 0.95 − 0.93 (m, 3H), 0.91 (s, 3H); ^{13}C NMR (150 MHz, $CDCl_3$) δ 199.4, 176.6, 164.9, 151.8, 151.2, 143.9, 130.3, 128.2, 125.6, 125.5, 121.3, 120.2, 112.2, 112.0, 70.6, 60.4, 59.0, 55.9, 48.8, 47.3, 46.5, 45.1, 43.8, 40.9, 39.2, 38.6, 37.5, 34.5, 34.2, 33.9, 33.1, 30.9, 28.8, 27.4, 27.1, 26.6, 25.0, 21.1, 20.5, 19.7, 18.2, 17.4, 13.1; HRMS (ESI$^+$) calcd. for $C_{40}H_{57}N_4O_4$ $[M + H]^+$ 657.2958 found 657.2956. Elemental analysis: $C_{40}H_{56}N_4O_4$ calcd.: C, 73.16; H, 8.57; N, 8.55; O, 9.72; found: C, 73.14; H, 8.59; N, 8.53; O, 9.74.

*5.4.5. N-((1-(4-bromophenyl)-1H-1,2,3-triazol-4-yl)methyl)-3α-hydroxy-11-oxours-12-en-24-carboxamide (**7e**).* Gummy red brown solid; Yield = 90%; ^{1}H NMR (600 MHz, $CDCl_3$) δ 8.05 (d, J = 1.8 Hz, 1H), 7.68 − 7.64 (m, 2H), 7.60 (d,

https://doi.org/10.1021/acsomega.5c01259
ACS Omega 2025, 10, 21715−21730

J = 8.5 Hz, 2H), 7.50 − 7.44 (m, 1H), 6.95 − 6.89 (m, 1H), 6.52 (s, 1H), 5.52 (s, 1H), 4.63 (d, J = 5.8 Hz, 1H), 4.59 (d, J = 5.7 Hz, 1H), 4.16 − 4.09 (m, 2H), 2.95 (q, J = 7.4 Hz, 4H), 2.81 (d, J = 1.2 Hz, 2H), 2.46 − 2.37 (m, 3H), 2.11 − 2.04 (m, 2H), 1.86 (d, J = 5.2 Hz, 1H), 1.81 − 1.76 (m, 2H), 1.70 (d, J = 4.6 Hz, 1H), 1.58 − 1.54 (m, 1H), 1.50 (dd, J = 11.2, 5.5 Hz, 3H), 1.48 − 1.43 (m, 1H), 1.30 (s, 3H), 1.28 (s, 3H), 1.21 (d, J = 4.3 Hz, 1H), 1.13 (s, 3H), 1.01 (d, J = 11.5 Hz, 1H), 0.90 (s, 3H), 0.80 (s, 3H), 0.78 (d, J = 6.5 Hz, 3H); ^{13}C NMR (150 MHz, $CDCl_3$) δ 199.3, 176.8, 165.0, 145.5, 135.8, 133.0, 132.7, 130.4, 121.9, 120.6, 70.6, 60.4, 59.0, 48.7, 47.3, 46.4, 45.0, 43.8, 40.9, 39.2, 38.6, 37.5, 34.6, 34.1, 33.9, 33.0, 30.9, 28.8, 27.4, 27.1, 26.6, 25.0, 21.0, 20.5, 19.6, 18.3, 17.4, 13.1; HRMS (ESI$^+$) calcd. for $C_{39}H_{54}{}^{79}BrN_4O_3$ $[M + H]^+$ 705.3574 found 705.3576. HRMS (ESI$^+$) calcd. for $C_{39}H_{54}{}^{81}BrN_4O_3$ $[M + H]^+$ 707.3566 found 707.3564. Elemental analysis: $C_{39}H_{53}BrN_4O_3$ calcd.: C, 66.39; H, 7.58; Br, 11.30; N, 7.96; O, 6.80; found: C, 66.37; H, 7.57; Br, 11.32; N, 7.94; O, 6.80.

*5.4.6. N-((1-(3-bromophenyl)-1H-1,2,3-triazol-4-yl)-methyl)-3α-hydroxy-11-oxours-12-en-24-carboxamide (**7f**).* Gummy red brown solid; Yield = 92%; ^{1}H NMR (600 MHz, $CDCl_3$) δ 7.92 (t, J = 2.0 Hz, 1H), 7.68 − 7.61 (m, 1H), 7.60 − 7.56 (m, 1H), 7.40 (t, J = 8.1 Hz, 1H), 7.29 − 7.27 (m, 1H), 7.22 (t, J = 8.0 Hz, 1H), 6.97 (ddd, J = 8.0, 2.2, 1.0 Hz, 1H), 6.64 (s, 1H), 5.51 (s, 1H), 4.67 (qd, J = 15.1, 5.5 Hz, 2H), 4.25 − 3.99 (m, 2H), 2.96 (d, J = 5.7 Hz, 4H), 2.81 (s, 2H), 2.46 − 2.34 (m, 3H), 2.05 (s, 2H), 1.86 (dt, J = 14.3, 7.1 Hz, 1H), 1.83 − 1.77 (m, 2H), 1.68 (dt, J = 16.9, 8.5 Hz, 1H), 1.59 − 1.54 (m, 1H), 1.52 − 1.47 (m, 3H), 1.46 − 1.42 (m, 1H), 1.29 (s, 3H), 1.26 (d, J = 1.7 Hz, 3H), 1.20 − 1.17 (m, 1H), 1.13 (s, 3H), 1.02 − 0.98 (m, 1H), 0.90 (s, 3H), 0.80 (s, 3H), 0.78 (d, J = 6.4 Hz, 3H); ^{13}C NMR (150 MHz, $CDCl_3$) δ 199.4, 176.9, 165.0, 145.5, 141.5, 137.7, 131.9, 130.4, 128.0, 123.6, 122.1, 118.9, 117.7, 70.5, 60.4, 59.0, 48.7, 47.4, 46.4, 45.0, 43.7, 40.9, 39.2, 38.6, 37.5, 34.6, 34.1, 33.9, 33.0, 30.9, 28.9, 27.4, 27.1, 26.6, 25.0, 21.1, 20.5, 19.6, 18.3, 17.4, 13.1; HRMS (ESI$^+$) calcd. for $C_{39}H_{54}{}^{79}BrN_4O_3$ $[M + H]^+$ 705.3292 found 705.3294. HRMS (ESI$^+$) calcd. for $C_{39}H_{54}{}^{81}BrN_4O_3$ $[M + H]^+$ 707.3290 found 707.3288. Elemental analysis: $C_{39}H_{53}BrN_4O_3$ calcd.: C, 66.35; H, 7.55; Br, 11.34; N, 7.92; O, 6.82; found: C, 66.37; H, 7.57; Br, 11.32; N, 7.94; O, 6.80.

*5.4.7. N-((1-(4-methoxyphenyl)-1H-1,2,3-triazol-4-yl)-methyl)-3α-hydroxy-11-oxours-12-en-24-carboxamide (**7g**).* Gummy black solid; Yield = 94%; ^{1}H NMR (600 MHz, $CDCl_3$) δ 7.96 (s, 1H), 7.63 − 7.56 (m, 2H), 7.04 − 7.01 (m, 2H), 6.98 (d, J = 2.3 Hz, 1H), 6.90 (d, J = 2.2 Hz, 1H), 6.51 (s, 1H), 5.53 (s, 1H), 4.64 (ddd, J = 47.6, 14.8, 5.6 Hz, 2H), 4.16 − 4.13 (m, 2H), 3.88 (s, 3H), 2.85 (d, J = 7.3 Hz, 2H), 2.82 (s, 3H), 2.49 − 2.42 (m, 3H), 2.07 (s, 3H), 1.88 (d, J = 5.1 Hz, 1H), 1.81 (d, J = 3.2 Hz, 2H), 1.71 (d, J = 8.8 Hz, 1H), 1.59 − 1.56 (m, 1H), 1.51 (d, J = 12.5 Hz, 3H), 1.48 − 1.45 (m, 1H), 1.32 (d, J = 3.9 Hz, 3H), 1.29 (d, J = 4.3 Hz, 3H), 1.20 (d, J = 2.1 Hz, 1H), 1.14 (s, 3H), 1.03 (d, J = 5.5 Hz, 1H), 0.92 (s, 3H), 0.81 (s, 3H), 0.80 (d, J = 6.5 Hz, 3H); ^{13}C NMR (150 MHz, $CDCl_3$) δ 199.3, 176.7, 171.1, 164.9, 159.9, 156.9, 144.9, 132.3, 130.5, 122.2, 120.0, 115.1, 114.8, 70.7, 60.4, 59.0, 55.5, 48.7, 47.3, 46.3, 45.0, 43.8, 40.9, 39.2, 38.6, 37.5, 34.6, 34.1, 33.9, 33.1, 30.9, 28.8, 27.5, 27.1, 26.6, 25.0, 21.1, 20.5, 19.6, 18.3, 17.4, 13.0; HRMS (ESI$^+$) calcd. for $C_{40}H_{57}N_4O_4$ $[M + H]^+$ 657.4590 found 657.4592. Elemental analysis: $C_{40}H_{56}N_4O_4$ calcd.: C, 73.16; H, 8.57; N, 8.55; O, 9.76; found: C, 73.14; H, 8.59; N, 8.53; O, 9.74.

*5.4.8. N-((1-(3-(trifluoromethyl)phenyl)-1H-1,2,3-triazol-4-yl)methyl)-3α-hydroxy-11-oxours-12-en-24-carboxamide (**7h**).* Gummy brown solid; Yield = 92%; ^{1}H NMR (600 MHz, $CDCl_3$) δ 8.17 (s, 1H), 8.02 (d, J = 2.1 Hz, 1H), 7.91 (dt, J = 8.0, 1.7 Hz, 1H), 7.70 (dt, J = 15.7, 7.8 Hz, 2H), 7.28 − 7.20 (m, 1H), 6.60 (t, J = 5.9 Hz, 1H), 5.51 (s, 1H), 4.66 (qd, J = 15.0, 5.8 Hz, 2H), 4.15 − 4.11 (m, 1H), 3.00 (q, J = 7.3 Hz, 4H), 2.81 (s, 2H), 2.47 − 2.35 (m, 3H), 2.11 − 2.01 (m, 2H), 1.87 (dd, J = 13.7, 5.2 Hz, 1H), 1.82 (ddt, J = 12.4, 9.1, 4.0 Hz, 3H), 1.70 (td, J = 11.4, 6.9 Hz, 1H), 1.59 − 1.54 (m, 1H), 1.53 − 1.47 (m, 4H), 1.46 − 1.43 (m, 1H), 1.29 (s, 3H), 1.27 (d, J = 2.9 Hz, 3H), 1.20 (dd, J = 8.0, 4.9 Hz, 1H), 1.13 (s, 3H), 1.02 − 0.99 (m, 1H), 0.91 (s, 3H), 0.80 (s, 3H), 0.78 (d, J = 6.4 Hz, 3H); ^{13}C NMR (150 MHz, $CDCl_3$) δ 199.4, 176.9, 165.0, 145.7, 141.0, 137.1, 132.5, 130.6, 130.4, 125.5, 123.5, 121.2, 117.5, 70.5, 60.4, 59.0, 48.7, 47.4, 46.5, 45.0, 43.8, 40.9, 39.2, 38.6, 37.5, 34.5, 34.1, 33.9, 33.0, 30.8, 28.8, 27.4, 27.1, 26.6, 25.0, 21.1, 20.5, 19.6, 18.3, 17.4, 13.1; ^{19}F NMR (564 MHz, $CDCl_3$) δ − 62.9; HRMS (ESI$^+$) calcd. for $C_{40}H_{54}F_3N_4O_3$ $[M + H]^+$ 695.4276 found 695.4278. Elemental analysis: $C_{40}H_{53}F_3N_4O_3$ calcd.: C, 69.16; H, 7.67; F, 8.22; N, 8.08; O, 6.93; found: C, 69.14; H, 7.69; F, 8.20; N, 8.06; O, 6.91.

*5.4.9. N-((1-(4-(trifluoromethyl)phenyl)-1H-1,2,3-triazol-4-yl)methyl)-3α-hydroxy-11-oxours-12-en-24-carboxamide (**7i**).* Gummy brown solid; Yield = 90%; ^{1}H NMR (600 MHz, $CDCl_3$) δ 8.13 (s, 1H), 7.87 (d, J = 8.4 Hz, 2H), 7.81 (d, J = 8.5 Hz, 2H), 7.62 (d, J = 8.4 Hz, 1H), 7.13 (d, J = 8.3 Hz, 1H), 6.48 (t, J = 5.8 Hz, 1H), 5.52 (s, 1H), 4.69 − 4.56 (m, 2H), 4.13 (t, J = 3.3 Hz, 1H), 2.99 (dd, J = 15.3, 8.0 Hz, 4H), 2.81 (s, 2H), 2.49 − 2.37 (m, 3H), 2.08 (s, 1H), 1.88 (dd, J = 13.7, 5.2 Hz, 1H), 1.86 − 1.74 (m, 3H), 1.71 (d, J = 4.8 Hz, 1H), 1.59 − 1.56 (m, 1H), 1.54 − 1.48 (m, 4H), 1.47 − 1.44 (m, 1H), 1.31 (s, 3H), 1.28 (s, 3H), 1.21 (dd, J = 11.3, 4.4 Hz, 1H), 1.13 (s, 3H), 1.03 − 1.00 (m, 1H), 0.90 (s, 3H), 0.81 (s, 3H), 0.78 (d, J = 6.4 Hz, 3H); ^{13}C NMR (150 MHz, $CDCl_3$) δ 199.3, 176.9, 165.0, 145.7, 139.2, 130.9, 130.4, 127.2, 120.9, 120.4, 119.2, 114.1, 70.6, 60.4, 59.0, 48.7, 47.4, 46.5, 45.0, 43.8, 40.9, 39.2, 38.6, 37.5, 34.6, 34.1, 33.9, 33.1, 30.9, 28.8, 27.4, 27.1, 26.5, 25.0, 21.1, 20.5, 19.6, 18.3, 17.4, 13.0; ^{19}F NMR (565 MHz, $CDCl_3$) δ − 62.6; HRMS (ESI$^+$) calcd. for $C_{40}H_{54}F_3N_4O_3$ $[M + H]^+$ 695.4557 found 695.4555. Elemental analysis: $C_{40}H_{53}F_3N_4O_3$ calcd.: C, 69.12; H, 7.70; F, 8.19; N, 8.05; O, 6.90; found: C, 69.14; H, 7.69; F, 8.20; N, 8.06; O, 6.91.

*5.4.10. N-((1-(4-fluorophenyl)-1H-1,2,3-triazol-4-yl)-methyl)-3α-hydroxy-11-oxours-12-en-24-carboxamide (**7j**).* Gummy dark brown solid; Yield = 92%; ^{1}H NMR (600 MHz, $CDCl_3$) δ 8.03 (s, 1H), 7.71 − 7.61 (m, 2H), 7.54 − 7.47 (m, 2H), 7.00 − 6.94 (m, 2H), 6.52 − 6.39 (m, 1H), 5.53 (s, 1H), 4.61 (ddd, J = 46.1, 15.1, 5.7 Hz, 2H), 4.17 − 4.11 (m, 1H), 2.89 − 2.86 (m, 4H), 2.82 (s, 3H), 2.48 − 2.38 (m, 4H), 1.90 − 1.85 (m, 1H), 1.80 (d, J = 6.3 Hz, 3H), 1.58 (s, 1H), 1.53 − 1.50 (m, 4H), 1.47 (d, J = 2.4 Hz, 1H), 1.31 (s, 3H), 1.28 (d, J = 3.0 Hz, 3H), 1.21 (d, J = 4.9 Hz, 1H), 1.14 (s, 3H), 1.02 (s, 1H), 0.91 (s, 3H), 0.81 (s, 3H), 0.79 (d, J = 6.5 Hz, 3H); ^{13}C NMR (150 MHz, $CDCl_3$) δ 199.3, 176.8, 164.9, 145.4, 138.6, 135.3, 134.7, 130.4, 130.2, 129.8, 121.7, 120.2, 116.2, 70.6, 60.4, 59.0, 48.7, 47.3, 46.3, 45.0, 43.8, 40.9, 39.2, 38.6, 37.5, 34.6, 34.1, 33.9, 33.1, 30.9, 28.8, 27.4, 27.1, 26.5, 25.0, 21.1, 20.5, 19.6, 18.3, 17.4, 13.0; ^{19}F NMR (564 MHz, $CDCl_3$) δ − 111.9; HRMS (ESI$^+$) calcd. for $C_{39}H_{54}FN_4O_3$ $[M + H]^+$ 645.3438 found 645.3436. Elemental analysis: $C_{39}H_{53}FN_4O_3$ calcd.: C, 72.66; H, 8.26; F, 2.97; N, 8.67; O, 7.42; found: C, 72.64; H, 8.28; F, 2.95; N, 8.69; O, 7.44.

*5.4.11. N-((1-(4-chlorophenyl)-1H-1,2,3-triazol-4-yl)-methyl)-3α-hydroxy-11-oxours-12-en-24-carboxamide (**7k**).* Gummy dark yellow solid; Yield = 90%; ^{1}H NMR (600 MHz,

https://doi.org/10.1021/acsomega.5c01259
ACS Omega 2025, 10, 21715−21730

$CDCl_3$) δ 8.02 (s, 1H), 7.71 − 7.64 (m, 2H), 7.26 − 7.20 (m, 2H), 7.09 − 7.05 (m, 1H), 7.03 − 6.98 (m, 1H), 6.52 (d, J = 6.0 Hz, 1H), 5.52 (s, 1H), 4.69 − 4.56 (m, 2H), 4.17 − 4.11 (m, 1H), 2.98 − 2.94 (m, 4H), 2.81 (s, 3H), 2.49 − 2.34 (m, 4H), 1.89 − 1.85 (m, 1H), 1.83 − 1.75 (m, 3H), 1.74 − 1.69 (m, 1H), 1.59 − 1.55 (m, 1H), 1.52 − 1.48 (m, 3H), 1.47 − 1.43 (m, 1H), 1.30 (d, J = 3.3 Hz, 3H), 1.29 (s, 3H), 1.21 (dd, J = 5.1, 2.1 Hz, 1H), 1.13 (s, 3H), 1.03 − 1.01 (m, 1H), 0.90 (s, 3H), 0.82 (s, 3H), 0.79 (d, J = 6.5 Hz, 3H); ^{13}C NMR (150 MHz, $CDCl_3$) δ 199.3, 176.8, 165.0, 163.3, 145.3, 133.1, 122.5, 121.3, 120.3, 116.8, 116.5, 70.6, 60.4, 59.0, 48.7, 47.3, 46.4, 45.0, 43.8, 40.9, 39.2, 38.6, 37.5, 34.6, 34.1, 33.9, 33.1, 30.9, 28.8, 27.4, 27.1, 26.6, 25.0, 21.1, 20.5, 19.6, 18.3, 17.4, 13.0; HRMS (ESI$^+$) calcd. for $C_{39}H_{54}ClN_4O_3$ [M + H]$^+$ 661.3677 found 661.3679. Elemental analysis: $C_{39}H_{53}ClN_4O_3$ calcd.: C, 70.85; H, 8.06; Cl, 5.34; N, 8.45; O, 7.28; found: C, 70.83; H, 8.08; Cl, 5.36; N, 8.47; O, 7.26.

*5.4.12. N-((1-phenyl-1H-1,2,3-triazol-4-yl)methyl)-3,11-dioxours-12-en-24-carboxamide (**8a**).* Gummy brown solid; Yield = 92%; ^{1}H NMR (600 MHz, $CDCl_3$) δ 8.02 (s, 1H), 7.71 (d, J = 8.0 Hz, 2H), 7.54 (d, J = 7.8 Hz, 2H), 7.46 (t, J = 7.2 Hz, 1H), 7.15 (t, J = 7.4 Hz, 1H), 7.04 (d, J = 8.0 Hz, 2H), 5.57 (s, 1H), 4.58 (d, J = 5.7 Hz, 2H), 3.40 (d, J = 7.2 Hz, 1H), 3.06 − 3.02 (m, 3H), 2.85 (d, J = 7.3 Hz, 3H), 1.95 − 1.85 (m, 3H), 1.66 (d, J = 7.7 Hz, 1H), 1.56 − 1.54 (m, 2H), 1.46 (d, J = 12.4 Hz, 2H), 1.39 (s, 4H), 1.31 (d, J = 6.0 Hz, 2H), 1.28 (s, 3H), 1.23 (s, 3H), 1.21 (d, J = 7.1 Hz, 3H), 1.03 (s, 1H), 0.96 (d, J = 5.1 Hz, 3H), 0.83 (s, 3H), 0.80 (s, 3H); ^{13}C NMR (150 MHz, $CDCl_3$) δ 211.0, 198.7, 173.3, 171.1, 165.4, 144.9, 139.9, 137.9, 130.3, 129.7, 128.9, 124.8, 120.5, 119.0, 60.4, 60.1, 59.0, 57.9, 56.6, 46.4, 44.8, 43.7, 40.8, 39.2, 37.2, 34.9, 33.9, 32.9, 30.8, 28.8, 27.2, 22.2, 21.0, 20.3, 18.3, 17.4, 13.5; HRMS (ESI$^+$) calcd. for $C_{39}H_{53}N_4O_3$ [M + H]$^+$ 625.3527 found 625.3525. Elemental analysis: $C_{39}H_{52}N_4O_3$ calcd.: C, 74.98; H, 8.41; N, 8.95; O, 7.69; found: C, 74.96; H, 8.39; N, 8.97; O, 7.68.

*5.4.13. N-((1-(2-(trifluoromethyl)phenyl)-1H-1,2,3-triazol-4-yl)methyl)-3,11-dioxours-12-en-24-carboxamide (**8b**).* Gummy dark reddish solid; Yield = 93%; ^{1}H NMR (600 MHz, $CDCl_3$) δ 7.90 − 7.87 (m, 1H), 7.84 (s, 1H), 7.78 − 7.70 (m, 3H), 7.52 (d, J = 7.8 Hz, 1H), 7.45 − 7.43 (m, 2H), 6.25 (s, 1H), 5.59 (s, 1H), 4.63 − 4.57 (m, 2H), 1.92 (d, J = 5.1 Hz, 2H), 1.85 (s, 1H), 1.66 (s, 1H), 1.57 (t, J = 3.3 Hz, 2H), 1.49 − 1.45 (m, 3H), 1.40 (s, 3H), 1.39 (d, J = 2.8 Hz, 3H), 1.36 (s, 1H), 1.32 (d, J = 7.5 Hz, 3H), 1.30 (s, 3H), 1.24 (d, J = 3.2 Hz, 3H), 1.18 − 1.15 (m, 4H), 1.04 (d, J = 6.6 Hz, 1H), 0.97 (d, J = 3.2 Hz, 3H), 0.85 (d, J = 7.1 Hz, 3H), 0.82 (d, J = 2.3 Hz, 3H); ^{13}C NMR (151 MHz, $CDCl_3$) δ 211.0, 198.7, 173.3, 171.1, 165.4, 144.9, 139.9, 137.9, 130.3, 129.7, 128.9, 124.8, 120.9, 120.5, 119.0, 60.4, 60.1, 59.0, 58.7, 57.9, 56.6, 46.4, 44.8, 43.7, 40.8, 39.2, 38.6, 37.2, 34.9, 33.9, 32.9, 30.8, 28.8, 27.4, 27.2, 22.2, 21.0, 20.3, 18.3, 17.4, 13.5; ^{19}F NMR (564 MHz, $CDCl_3$) δ − 61.87; HRMS (ESI$^+$) calcd. for $C_{40}H_{52}F_3N_4O_3$ [M + H]$^+$ 693.6125 found 693.6128. Elemental analysis: $C_{40}H_{51}F_3N_4O_3$ calcd C, 69.36; H, 7.45; F, 8.21; N, 8.07; O, 6.93; found: C, 69.34; H, 7.42; F, 8.23; N, 8.09; O, 6.93.

*5.4.14. N-((1-(o-tolyl)-1H-1,2,3-triazol-4-yl)methyl)-3,11-dioxours-12-en-24-carboxamide (**8c**).* Gummy dark yellow solid; Yield = 96%; ^{1}H NMR (600 MHz, MeOD) δ 8.43 (d, J = 9.7 Hz, 1H), 7.78 (q, J = 8.3 Hz, 4H), 7.54 (d, J = 8.2 Hz, 1H), 7.03 (d, J = 8.2 Hz, 1H), 5.55 (s, 1H), 4.56 (s, 2H), 3.64 (d, J = 7.3 Hz, 1H), 3.55 (d, J = 6.4 Hz, 1H), 3.09 (s, 3H), 2.90 (s, 6H), 2.74 (s, 1H), 2.50 (s, 1H), 2.54−2.21 (m, 2H), 2.04 (s, 1H), 1.93 (dd, J = 40.3, 13.9 Hz, 4H), 1.65 (d, J = 32.9 Hz, 3H), 1.58 − 1.50 (m, 3H), 1.46 (d, J = 12.3 Hz, 5H), 1.26 (s, 3H), 1.11 (s, 1H), 1.05 (d, J = 9.0 Hz, 3H), 0.84 (s, 3H), 0.81 (d, J = 7.4 Hz, 3H); ^{13}C NMR (150 MHz, $CDCl_3$) δ 211.0, 199.3, 176.7, 164.9, 144.3, 136.2, 133.6, 131.5, 131.1, 127.0, 125.9, 124.5, 117.8, 70.6, 60.4, 59.0, 48.7, 47.3, 46.3, 45.0, 43.8, 40.9, 39.2, 38.6, 37.5, 33.9, 33.0, 30.9, 28.8, 27.4, 25.1, 21.1, 20.5, 19.7, 18.2, 17.8, 17.4, 14.2; HRMS (ESI$^+$) calcd. for $C_{40}H_{55}N_4O_3$ [M + H]$^+$ 639.4055 found 639.4052. Elemental analysis: $C_{40}H_{54}N_4O_3$ calcd C, 75.22; H, 8.54; N, 8.75; O, 7.53; found: C, 75.20; H, 8.52; N, 8.77; O, 7.51.

*5.4.15. N-((1-(2-methoxyphenyl)-1H-1,2,3-triazol-4-yl)-methyl)-3,11-dioxours-12-en-24-carboxamide (**8d**).* Gummy brown solid; Yield = 94%; ^{1}H NMR (600 MHz, $CDCl_3$) δ 7.97 (s, 1H), 7.76 (d, J = 10.0 Hz, 1H), 7.54 − 7.50 (m, 2H), 7.38 (s, 1H), 7.03 (s, 1H), 6.62 (s, 1H), 5.82 (d, J = 10.2 Hz, 1H), 5.53 (d, J = 23.8 Hz, 1H), 4.37 (d, J = 12.6 Hz, 2H), 3.81 (s, 3H), 2.32 (s, 2H), 1.92 (s, 1H), 1.87 (s, 2H), 1.62 (s, 3H), 1.53 − 1.45 (m, 4H), 1.32 (d, J = 4.2 Hz, 3H), 1.26 (d, J = 16.4 Hz, 2H), 1.15 (s, 4H), 1.13 (d, J = 3.5 Hz, 1H), 1.11 (s, 2H), 1.09 (d, J = 1.6 Hz, 3H), 1.07 − 1.02 (m, 3H), 0.96 (s, 1H), 0.89 (s, 3H), 0.78 (s, 3H), 0.74 (d, J = 6.4 Hz, 3H); ^{13}C NMR (150 MHz, $CDCl_3$) δ 211.1, 199.5, 176.6, 164.9, 151.8, 151.2, 143.9, 130.3, 128.2, 125.6, 125.5, 121.3, 120.2, 112.2, 112.0, 60.4, 59.0, 55.9, 48.8, 47.3, 46.5, 45.1, 43.8, 40.9, 39.2, 38.6, 37.5, 34.5, 34.2, 33.9, 33.1, 30.9, 28.8, 27.4, 27.1, 26.6, 25.0, 21.1, 20.5, 19.7, 18.2, 17.4, 13.1; HRMS (ESI$^+$) calcd. for $C_{40}H_{55}N_4O_4$ [M + H]$^+$ 655.3758 found 655.3761. Elemental analysis: $C_{40}H_{54}N_4O_4$ calcd C, 73.38; H, 8.33; N, 8.55; O, 9.75; found: C, 73.36; H, 8.31; N, 8.56; O, 9.77.

*5.4.16. N-((1-(4-bromophenyl)-1H-1,2,3-triazol-4-yl)-methyl)-3,11-dioxours-12-en-24-carboxamide (**8e**).* Gummy pale yellow solid; Yield = 92%; ^{1}H NMR (600 MHz, MeOD) δ 8.42 (d, J = 9.7 Hz, 1H), 7.77 (q, J = 8.3 Hz, 4H), 7.53 (d, J = 8.2 Hz, 1H), 7.02 (d, J = 8.2 Hz, 1H), 5.57 (s, 1H), 4.55 (s, 2H), 3.63 (d, J = 7.3 Hz, 1H), 3.54 (d, J = 6.4 Hz, 1H), 3.08 (s, 3H), 2.89 (s, 6H), 2.73 (s, 1H), 2.49 (s, 1H), 2.54−2.22 (m, 2H), 2.03 (s, 1H), 1.92 (dd, J = 40.3, 13.9 Hz, 4H), 1.64 (d, J = 32.9 Hz, 3H), 1.58 − 1.51 (m, 3H), 1.47 (d, J = 12.3 Hz, 5H), 1.11 (s, 1H), 1.06 (d, J = 9.0 Hz, 3H), 0.85 (s, 3H), 0.82 (d, J = 7.4 Hz, 3H); ^{13}C NMR (150 MHz, $CDCl_3$) δ 210.6, 199.3, 176.8, 165.0, 145.5, 135.8, 133.0, 132.7, 130.4, 121.9, 120.6, 60.4, 59.0, 48.7, 47.3, 46.4, 45.0, 43.8, 40.9, 39.2, 38.6, 37.5, 34.6, 34.1, 33.9, 33.0, 30.9, 28.8, 27.4, 27.1, 26.6, 25.0, 21.0, 20.5, 19.6, 18.3, 17.4, 13.1; HRMS (ESI$^+$) calcd. for $C_{39}H_{52}{}^{79}BrN_4O_3$ [M + H]$^+$ 703.3095 found 703.3092. HRMS (ESI$^+$) calcd. for $C_{39}H_{52}{}^{81}BrN_4O_3$ [M + H]$^+$ 705.3081 found 705.3083. Elemental analysis: $C_{39}H_{51}BrN_4O_3$ calcd.: C, 66.58; H, 7.32; N, 7.98; O, 6.85; found: C, 66.56; H, 7.30; N, 7.96; O, 6.82.

*5.4.17. N-((1-(3-bromophenyl)-1H-1,2,3-triazol-4-yl)-methyl)-3,11-dioxours-12-en-24-carboxamide (**8f**).* Gummy pale yellow solid; Yield = 93%; ^{1}H NMR (600 MHz, $CDCl_3$) δ 8.01 (s, 1H), 7.94 (t, J = 2.0 Hz, 1H), 7.66 (dd, J = 2.1, 0.9 Hz, 1H), 7.59 (ddd, J = 8.1, 1.9, 0.9 Hz, 1H), 7.42 (d, J = 8.1 Hz, 1H), 7.29 (dd, J = 1.8, 1.0 Hz, 1H), 6.30 (s, 1H), 5.58 (s, 1H), 4.57 (s, 2H), 2.44 − 2.38 (m, 2H), 2.18 − 2.10 (m, 3H), 1.86 − 1.83 (m, 1H), 1.58 − 1.55 (m, 2H), 1.46 (d, J = 6.6 Hz, 2H), 1.40 (s, 3H), 1.38 − 1.34 (m, 5H), 1.32 (d, J = 3.1 Hz, 3H), 1.24 (s, 4H), 1.23 (s, 3H), 1.18 − 1.13 (m, 3H), 1.03 (d, J = 6.5 Hz, 1H), 0.96 (d, J = 4.3 Hz, 3H), 0.84 (s, 3H), 0.80 (d, J = 6.5 Hz, 3H); ^{13}C NMR (150 MHz, $CDCl_3$) δ 211.1, 199.4, 176.9, 165.0, 145.5, 141.5, 137.7, 131.9, 130.4, 128.0, 123.6, 122.1, 118.9, 117.7, 60.4, 59.0, 48.7, 47.4, 46.4, 45.0, 43.7, 40.9, 39.2, 38.6, 37.5, 34.6, 34.1, 33.9, 33.0, 30.9, 28.9, 27.4 27.1, 26.6, 25.0, 21.1, 20.5, 19.6, 18.3, 17.4, 13.1; HRMS (ESI$^+$) calcd. for

https://doi.org/10.1021/acsomega.5c01259
ACS Omega 2025, 10, 21715−21730

$C_{39}H_{52}{}^{79}BrN_4O_3$ $[M + H]^+$ 703.3517 found 703.3519. HRMS (ESI^+) calcd. for $C_{39}H_{52}{}^{81}BrN_4O_3$ $[M + H]^+$ 705.3511 found 705.3509. Elemental analysis: $C_{39}H_{51}BrN_4O_3$ calcd.: C, 66.54; H, 7.28; N, 7.98; O, 6.80; found: C, 66.56; H, 7.30; N, 7.96; O, 6.82.

*5.4.18. N-((1-(4-methoxyphenyl)-1H-1,2,3-triazol-4-yl)-methyl)-3,11-dioxours-12-en-24-carboxamide (**8g**).* Gummy dark brown solid; Yield = 96%; ^1H NMR (600 MHz, $CDCl_3$) δ 7.98 (s, 1H), 7.77 (d, J = 10.0 Hz, 1H), 7.54 − 7.51 (m, 2H), 7.37 (s, 1H), 7.02 (s, 1H), 6.61 (s, 1H), 5.81 (d, J = 10.2 Hz, 1H), 5.51 (d, J = 23.8 Hz, 1H), 4.36 (d, J = 12.6 Hz, 2H), 3.80 (s, 3H), 2.31 (s, 2H), 1.91 (s, 1H), 1.86 (s, 2H), 1.60 (s, 3H), 1.53 − 1.47 (m, 4H), 1.31 (d, J = 4.2 Hz, 3H), 1.27 (d, J = 16.4 Hz, 2H), 1.14 (s, 4H), 1.12 (d, J = 3.5 Hz, 1H), 1.10 (s, 2H), 1.08 (d, J = 1.6 Hz, 3H), 1.07 − 1.07 (m, 3H), 0.95 (s, 1H), 0.88 (s, 3H), 0.77 (s, 3H), 0.73 (d, J = 6.4 Hz, 3H); ^{13}C NMR (150 MHz, $CDCl_3$) δ 211.0, 199.3, 176.7, 171.1, 164.9, 159.9, 156.9, 144.9, 132.3, 130.5, 122.2, 120.0, 115.1, 114.8, 60.4, 59.0, 55.5, 48.7, 47.3, 46.3, 45.0, 43.8, 40.9, 39.2, 38.6, 37.5, 34.6, 34.1, 33.9, 33.1, 30.9, 28.8, 27.5, 27.1, 26.6, 25.0, 21.1, 20.5, 19.6, 18.3, 17.4, 14.2; HRMS (ESI^+) calcd. for $C_{40}H_{55}N_4O_4$ $[M + H]^+$ 655.4327 found 655.4329. Elemental analysis: $C_{40}H_{54}N_4O_4$ calcd.: C, 73.38; H, 8.33; N, 8.54; O, 9.75; found: C, 73.36; H, 8.31; N, 8.56; O, 9.77.

*5.4.19. N-((1-(3-(trifluoromethyl)phenyl)-1H-1,2,3-triazol-4-yl)methyl)-3,11-dioxours-12-en-24-carboxamide (**8h**).* Gummy red brown solid; Yield = 92%; ^1H NMR (600 MHz, $CDCl_3$) δ 8.10 (s, 1H), 8.03 (d, J = 4.6 Hz, 1H), 7.93 (s, 1H), 7.72 (t, J = 8.4 Hz, 2H), 7.50 (d, J = 7.9 Hz, 1H), 7.42 (s, 2H), 6.38 (s, 1H), 5.59 (d, J = 21.3 Hz, 1H), 4.59 (d, J = 5.9 Hz, 2H), 2.39 (d, J = 14.8 Hz, 3H), 2.13 (d, J = 12.7 Hz, 2H), 1.98 − 1.80 (m, 4H), 1.66 (s, 1H), 1.57 (s, 2H), 1.50 (dd, J = 13.9, 10.9 Hz, 4H), 1.35 (s, 2H), 1.29 (s, 3H), 1.24 (s, 2H), 1.21 (s, 3H), 1.18 − 1.14 (m, 3H), 1.03 (s, 1H), 0.96 (d, J = 4.4 Hz, 3H), 0.84 (s, 3H), 0.81 − 0.79 (m, 3H); ^{13}C NMR (150 MHz, $CDCl_3$) δ 211.1, 199.4, 176.9, 165.0, 145.7, 141.0, 137.1, 132.5, 130.6, 130.4, 125.5, 123.5, 121.2, 117.5, 60.4, 59.0, 48.7, 47.4, 46.5, 45.0, 43.8, 40.9, 39.2, 38.6, 37.5, 34.5, 34.1, 33.9, 33.0, 30.8, 28.83, 27.4, 27.1, 26.6, 25.0, 21.1, 20.5, 19.6, 18.3, 17.4, 13.1; ^{19}F NMR (564 MHz, $CDCl_3$) δ − 62.9; HRMS (ESI^+) calcd. for $C_{40}H_{52}F_3N_4O_3$ $[M + H]^+$ 693.5551 found 693.5549. Elemental analysis: $C_{40}H_{51}F_3N_4O_3$ calcd.: C, 69.32; H, 7.44; N, 8.11; O, 6.95; found: C, 69.34; H, 7.42; N, 8.09; O, 6.93.

*5.4.20. N-((1-(4-(trifluoromethyl)phenyl)-1H-1,2,3-triazol-4-yl)methyl)-3,11-dioxours-12-en-24-carboxamide (**8i**).* Gummy pale yellow solid; Yield = 94%; ^1H NMR (600 MHz, $CDCl_3$) δ 8.05 (s, 1H), 7.80 (d, J = 8.3 Hz, 2H), 7.72 (d, J = 8.4 Hz, 2H), 7.31 (t, J = 7.8 Hz, 1H), 7.21 (s, 1H), 6.38 (t, J = 5.8 Hz, 1H), 5.48 (s, 1H), 4.52 (d, J = 5.9 Hz, 2H), 2.36 − 2.26 (m, 3H), 2.02 (dd, J = 13.7, 4.5 Hz, 2H), 1.87 − 1.74 (m, 4H), 1.58 (s, 1H), 1.47 (dd, J = 7.8, 3.6 Hz, 2H), 1.42 − 1.36 (m, 4H), 1.31 (s, 3H), 1.27 (d, J = 1.6 Hz, 2H), 1.24 (d, J = 7.0 Hz, 2H), 1.20 (s, 3H), 1.09 (s, 1H), 1.04 (t, J = 7.1 Hz, 3H), 0.94 (dd, J = 5.9, 3.3 Hz, 1H), 0.87 (s, 3H), 0.74 (s, 3H), 0.71 (d, J = 6.5 Hz, 3H); ^{13}C NMR (150 MHz, $CDCl_3$) δ 211.0, 199.3, 176.9, 165.0, 145.7, 139.2, 130.9, 130.4, 127.2, 120.9, 120.4, 119.2, 114.1, 60.4, 59.0, 48.7, 47.4, 46.5, 45.0, 43.8, 40.9, 39.2, 38.6, 37.5, 34.6, 34.1, 33.9, 33.1, 30.9, 28.8, 27.4, 27.1, 26.5, 25.0, 21.1, 20.5, 19.6, 18.3, 17.4, 13.0; ^{19}F NMR (564 MHz, $CDCl_3$) δ − 62.2; HRMS (ESI^+) calcd. for $C_{40}H_{52}F_3N_4O_3$ $[M + H]^+$ 693.5026 found 693.5028. Elemental analysis: $C_{40}H_{51}F_3N_4O_3$ calcd.: C, 69.36; H, 7.40; N, 8.07; O, 6.91; found: C, 69.34; H, 7.42; N, 8.09; O, 6.93.

*5.4.21. N-((1-(4-fluorophenyl)-1H-1,2,3-triazol-4-yl)-methyl)-3,11-dioxours-12-en-24-carboxamide (**8j**).* Gummy red brown solid; Yield = 93%; ^1H NMR (600 MHz, $CDCl_3$) δ 7.97 (s, 1H), 7.69 (ddd, J = 9.1, 4.6, 2.6 Hz, 4H), 6.97 − 6.79 (m, 1H), 6.65 (dd, J = 16.0, 9.6 Hz, 1H), 6.30 (d, J = 6.1 Hz, 1H), 5.58 (s, 1H), 4.56 (d, J = 5.7 Hz, 2H), 2.44 − 2.37 (m, 3H), 2.11 (d, J = 14.4 Hz, 3H), 1.92 (dd, J = 13.1, 5.7 Hz, 2H), 1.85 (s, 1H), 1.66 (s, 1H), 1.57 − 1.54 (m, 4H), 1.50 − 1.48 (m, 2H), 1.40 (s, 3H), 1.35 (d, J = 2.6 Hz, 3H), 1.26 (s, 3H), 1.20 (d, J = 1.7 Hz, 2H), 1.14 (s, 3H), 1.03 (d, J = 2.9 Hz, 1H), 0.96 (s, 3H), 0.84 (s, 3H), 0.80 (d, J = 6.5 Hz, 3H); ^{13}C NMR (150 MHz, $CDCl_3$) δ 211.1, 199.3, 176.8, 164.9, 145.4, 138.6, 135.3, 134.7, 130.5, 130.2, 129.8, 121.7, 120.2, 116.2, 60.4, 59.0, 48.7, 47.3, 46.3, 45.0, 43.8, 40.9, 39.2, 38.6, 37.5, 34.6, 34.1, 33.9, 33.1, 30.9, 28.8, 27.4, 27.1, 26.5, 25.0, 21.1, 20.5, 19.6, 18.3, 17.4, 13.0; ^{19}F NMR (564 MHz, $CDCl_3$) δ − 117.7; HRMS (ESI^+) calcd. for $C_{39}H_{52}FN_4O_3$ $[M + H]^+$ 643.4223 found 643.4225. Elemental analysis: $C_{39}H_{51}FN_4O_3$ calcd.: C, 72.66; H, 8.26; F, 2.97; N, 8.67; O, 7.42; found: C, 72.87; H, 8.00; F, 2.96; N, 8.72; O, 7.47.

*5.4.22. N-((1-(4-chlorophenyl)-1H-1,2,3-triazol-4-yl)-methyl)-3,11-dioxours-12-en-24-carboxamide (**8k**).* Gummy dark brown solid; Yield = 92%; ^1H NMR (600 MHz, $CDCl_3$) δ 7.99 (s, 1H), 7.67 (d, J = 7.7 Hz, 2H), 7.52 (d, J = 8.8 Hz, 2H), 7.11 (d, J = 8.6 Hz, 1H), 6.62 (d, J = 8.4 Hz, 1H), 6.28 (s, 1H), 5.58 (s, 1H), 4.56 (d, J = 5.6 Hz, 2H), 2.43 − 2.37 (m, 3H), 2.13 − 2.10 (m, 2H), 1.96 − 1.90 (m, 2H), 1.84 (d, J = 14.3 Hz, 1H), 1.66 (s, 1H), 1.56 (d, J = 10.3 Hz, 2H), 1.53 − 1.47 (m, 5H), 1.40 (s, 3H), 1.35 (d, J = 3.2 Hz, 2H), 1.33 (s, 3H), 1.26 (s, 3H), 1.16 (d, J = 5.3 Hz, 3H), 1.03 (d, J = 6.4 Hz, 1H), 0.96 (s, 3H), 0.84 (s, 3H), 0.80 (d, J = 6.4 Hz, 3H); ^{13}C NMR (150 MHz, $CDCl_3$) δ 211.0, 199.3, 176.8, 165.0, 163.3, 145.3, 133.1, 122.5, 121.3, 120.3, 116.8, 116.5, 60.4, 59.0, 48.7, 47.3, 46.4, 45.0, 43.8, 40.9, 39.2, 38.6, 37.5, 34.6, 34.1, 33.9, 33.1, 30.9, 28.8, 27.4, 27.1, 26.6, 25.0, 21.1, 20.5, 19.6, 18.3, 17.4, 13.0; HRMS (ESI^+) calcd. for $C_{39}H_{52}ClN_4O_3$ $[M + H]^+$ 659.3812 found 659.3810. Elemental analysis: $C_{39}H_{51}ClN_4O_3$ calcd.: C, 71.07; H, 7.82; N, 8.52; O, 7.26; found: C, 71.05; H, 7.80; N, 8.50; O, 7.28.

5.5. Cell Culture and Experimental Conditions. Human breast cancer cell lines, MDA-MB-231 (metastatic) and MCF-7 (nonmetastatic), along with Human Dermal Fibroblast (HDF) cells, were obtained from the American Type Culture Collection (ATCC; Manassas, VA, USA). MDA-MB-231 and MCF-7 cells were cultured in high-glucose DMEM (Dulbecco's Modified Eagle Medium) supplemented with 1% penicillin-streptomycin and 10% fetal bovine serum (FBS), while HDF cells were cultured in RPMI 1640 medium, also supplemented with 1% penicillin-streptomycin and 10% FBS. All media and cell culture supplements were obtained from GIBCO (Thermo Fisher Scientific, USA). The cells were maintained in a humidified incubator set to 95% humidity at 37 °C with 5% CO_2. Stock solutions of each compound (200 mM) were prepared in DMSO and subsequently diluted to desired concentrations in complete culture media, ranging from 5−200 μM.

5.6. Assessment of Anti-proliferative Activity of Compounds on Breast Cancer and Normal Cells. The antiproliferative activity of the compounds on MDA-MB-231, MCF-7, and HDF cells was evaluated using the MTT assay. Cells were seeded in 96-well plates at a density of 1×10^4 cells per well and allowed to adhere for 24 h. Following this incubation, cells were treated with a range of 25 different compounds at concentrations of 5−200 μM for an additional 24 h. After the treatment period, MTT solution (5 mg/mL in PBS; Abcam, UK) was added to each well, and plates were incubated

https://doi.org/10.1021/acsomega.5c01259
ACS Omega 2025, 10, 21715−21730

at 37 °C for 3 h. The resulting formazan crystals were dissolved in DMSO, allowing for absorbance measurements at 570 nm using an xMark microplate reader (Bio-Rad Laboratories, Hercules, CA, USA). The antiproliferative effects were quantified as a percentage of cell viability relative to untreated control cells, and the IC50 values were evaluated as previously described.[55] Each assay was performed in triplicates, and results were expressed as mean ± standard deviation.

5.6.1. Peripheral Blood Mononuclear Cell (PBMC) Isolation and Treatments. PBMCs were isolated from whole blood samples obtained from six healthy volunteers using Histopaque-1077 (Sigma-Aldrich, St. Louis, MO, USA) and centrifugation, as previously described.[56−59] PBMCs were then resuspended in RPMI-1640 medium (Gibco) supplemented with 10% FBS (Gibco), 1% penicillin-streptomycin (Gibco), and counted using LUNA-FL (Logos Biosystems, South Korea) to adjust the cell concentration to 1×10^6 cells/mL. The isolated PBMCs were seeded in 6-well plates and treated with the 7f derivative of KBA at concentrations of 5 μM, and 10 μM, based on prior cytotoxicity assessment results. Control (NC) wells received vehicle treatment (DMSO at a final concentration of 0.1% v/v). After 1 h of treatment, cells were activated by adding Concanavalin A (Con A) (Sigma-Aldrich, USA) at a final concentration of 5 μg/mL to induce T cell activation. After 24 h of incubation, cells were harvested and prepared for flow cytometric analysis.

5.6.2. Flow Cytometry Analysis. The harvested PBMCs were stained with CD3 (PerCP-Cyanine5.5, eBioscience: 45−0036−42), CD4 (PE-Cyanine7, eBioscience: 25−0049−42), CD8a (Super Bright 702, eBioscience: 67−0086−42), CD279 (PD-1) (PE-Cyanine5, eBioscience: 15−2799−42), and TIGIT (PE-eFluor 610, eBioscience: 61−9500−42) monoclonal antibodies. Prior to staining, cells were incubated with an Fc receptor blocking reagent (eBioscience, USA) to eliminate nonspecific bindings. Isotype controls, compensation controls, and a fluorescence minus one (FMO) control were employed. Data acquisition was performed using an Aurora Cytek Northern flow cytometer (Cytek Biosciences, USA). Data analysis was conducted using FlowJo X software (Tree Star, Ashland, Oregon, USA). Gating strategies were implemented to identify and quantify CD3+, CD4+, CD8+, PD-1+, and TIGIT+ populations. All experiments were performed in triplicate, and results were expressed as the percentage of positive cells within the defined gates.

5.7. Molecular Docking Studies. The X-ray crystal structure of human CDK4 in complex with Cyclin D3 and a ligand (abemaciclib) with a resolution of 2.51 Å, was taken from RCSB Protein Databank (PDB ID: 7SJ3). The protein structure was then optimized by Molecular Operating Environment (MOE 2024.06)[60] by adding proton and charges (through AMBER14:EHT force field) and saved into 'moe' format to be used in docking analysis. The structures of compounds **7b−7j** were generated on MOE, and AM1-BCC charges were added on each molecule, and their structures were minimized with MMFF94x force field with gradient of 0.1 kcal/mol/Å. Before docking our molecules, we tested the efficiency of MOE's induced fit docking protocol (Triangle Matcher docking algorithm and London dG scoring function in combination with GBVI/WSA dG refinement method) by redocking of cocrystallized cancer drug named abemaciclib with 100 conformations. In the redocking, abemaciclib was docked accurately at its binding site with RMSD of 1.52 Å and docking score of − 9.40 kcal/mol. In the active site, Lys35 and Val96 mediated hydrogen bonding with abemaciclib (at 2.90 Å and 2.87 Å), while Asp99 formed an ionic interaction (at 2.50 Å and 3.11 Å) with this drug, and Phe93 and Asp158 provided hydrophobic interactions (at 3.19 Å and 3.75 Å) to abemaciclib. The good redocking result (Figure 7) encouraged us to apply the same configuration of docking protocol to dock compounds **7b−7j** in the abemaciclib binding site of CDK-4 with 50 conformations of each molecule.

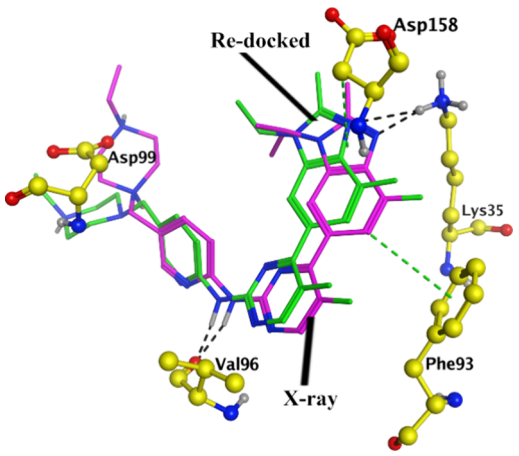

Figure 7. Binding mode of abemaciclib (magenta sticks model) is shown in the binding cavity of CDK-4. The interacting residues are depicted in yellow ball and stick model. The redocked conformation (green sticks) is superimposed on its X-ray conformation with RMSD of 1.52 Å. Hydrogen bonds and hydrophobic interactions are shown in black and green dashed lines, respectively.

■ ASSOCIATED CONTENT

Data Availability Statement

The data that has been used is confidential and necessary data is provided in the Supporting Information.

Supporting Information

The Supporting Information is available free of charge at https://pubs.acs.org/doi/10.1021/acsomega.5c01259.

H NMR, ^{13}C NMR, ^{19}F-NMR, and HR-ESI-MS spectra of compounds **4**, **5**, **7a−7k**, and **8a−8k** (PDF)

Crystallographic structures (CIF)

■ AUTHOR INFORMATION

Corresponding Authors

Satya Kumar Avula − *Natural & Medical Sciences Research Center, University of Nizwa, Nizwa 616, Oman;* orcid.org/0000-0003-3941-7164; Phone: +96825446328; Email: chemisatya@unizwa.edu.om

Ahmed Al-Harrasi − *Natural & Medical Sciences Research Center, University of Nizwa, Nizwa 616, Oman;* orcid.org/0000-0002-0815-5942; Phone: +96825446328; Email: aharrasi@unizwa.edu.om

Authors

Najeeb Ur Rehman − *Natural & Medical Sciences Research Center, University of Nizwa, Nizwa 616, Oman*

Hassan Moghtaderi − *Natural & Medical Sciences Research Center, University of Nizwa, Nizwa 616, Oman*

Saeed Mohammadi − *Natural & Medical Sciences Research Center, University of Nizwa, Nizwa 616, Oman*

Sadiq Noor Khan − *Natural & Medical Sciences Research Center, University of Nizwa, Nizwa 616, Oman*
Sobia Ahsan Halim − *Natural & Medical Sciences Research Center, University of Nizwa, Nizwa 616, Oman;* orcid.org/0000-0001-8526-7799
Muhammad U. Anwar − *Natural & Medical Sciences Research Center, University of Nizwa, Nizwa 616, Oman;* orcid.org/0000-0003-4740-5737
Shaikh Mizanoor Rahman − *Natural & Medical Sciences Research Center, University of Nizwa, Nizwa 616, Oman;* orcid.org/0000-0002-4879-2663
Simon Gibbons − *Natural & Medical Sciences Research Center, University of Nizwa, Nizwa 616, Oman;* orcid.org/0000-0003-1587-6809
René Csuk − *Organic Chemistry, Martin-Luther-University Halle-Wittenberg, Halle D-06120, Germany;* orcid.org/0000-0001-7911-290X

Complete contact information is available at: https://pubs.acs.org/10.1021/acsomega.5c01259

Author Contributions

N.U.R.: isolation, writing the original draft and validation. S.N.K.: synthesis. H.M., S.M., S.M.R.: biological evaluation, conceptualization. S.A.H.: molecular docking studies. M.U.A.: X-ray crystallography studies. S.G., R.C.: writing, reviewing and editing the manuscript, resources. S.K.A.: synthesis, project administration, writing original draft. A.A.H.: project administration, supervision, resources, writing (review and editing) of the manuscript.

Notes

The authors declare no competing financial interest.

■ ACKNOWLEDGMENTS

The University of Nizwa (UoN) kindly provided funding for this endeavor, which the authors gratefully acknowledge. The Minister of Higher Education, Research and Innovation financed this research through the project **BFP/RGP/CBS/21/006**. We greatly appreciate the help from the technical and analytical staff of UoN.

■ REFERENCES

(1) Zainab; Khan, F.; Alam, A.; Rehman, N. U.; Ullah, S.; Elhenawy, A. A.; Ali, M.; Islam, W. U.; Khan, A.; Al-Harrasi, A.; Ahmad, M.; Haitao, Y. Synthesis, anticancer, α-glucosidase inhibition, molecular docking and dynamics studies of hydrazone-Schiff bases bearing polyhydroquinoline scaffold: In vitro and in silico approaches. *J. Mol. Struct.* **2025**, *1321*, No. 139699.
(2) Lee, M. M.L.; Chan, B. D.; Wong, W.-Y.; Leung, T. W.; Qu, Z.; Huang, J.; Zhu, L.; Lee, C. S.; Chen, S.; Tai, W. C.-S. Synthesis and evaluation of novel anticancer compounds derived from the natural product Brevilin A. *ACS Omega.* **2020**, *5* (24), 14586−14596.
(3) Bray, F.; Ferlay, J.; Soerjomataram, I.; Siegel, R. L.; Torre, L. A.; Jemal, A. Global cancer statistics 2018: GLOBOCAN estimates of incidence and mortality worldwide for 36 cancers in 185 countries. *Cancer J. Clin.* **2018**, *68* (6), 394−424.
(4) Alam, A.; Khan, F.; Rehman, N. U.; Zainab; Elhenawy, A. A.; Islam, W. U.; Ali, M.; Aziz, S.; Al-Harrasi, A.; Ahmad, M. Flurbiprofen clubbed schiff's base derivatives as potent anticancer agents: In Vitro and In Silico approach towards breast cancer. *J. Mol. Struct.* **2025**, *1321*, No. 139743.
(5) Ibrahim, N. S. M.; Kadry, H. H.; Zaher, A. F.; Mohamed, K. O. Synthesis and anticancer activity of pyrimido [4, 5-b] quinolines in the last twenty years. *Chem. Pap.* **2024**, *78* (5), 2729−2755.
(6) Abd El-Meguid, E.; Awad, H.; Anwar, M. Synthesis of new 1, 3, 4-oxadiazole-benzimidazole derivatives as potential antioxidants and breast cancer inhibitors with apoptosis inducing activity. *Russ. J. Gen. Chem.* **2019**, *89*, 348−356.
(7) Liu, J.; Ming, B.; Gong, G. H.; Wang, D.; Bao, G. L.; Yu, L.-J. Current research on anti-breast cancer synthetic compounds. *RSC advances.* **2018**, *8* (8), 4386−4416.
(8) Bentley, G.; Zamir, O.; Dahabre, R.; Perry, S.; Karademas, E. C.; Poikonen-Saksela, P.; Mazzocco, K.; Sousa, B.; Pat-Horenczyk, R. Protective Factors against Fear of Cancer Recurrence in Breast Cancer Patients: A latent growth model. protective factors against fear of cancer recurrence in breast cancer patients: a latent growth model. *Cancers.* **2023**, *15* (18), 4590.
(9) Blyth, R. R. R.; Birts, C. N.; Beers, S. A. The role of three-dimensional in vitro models in modelling the inflammatory micro-environment associated with obesity in breast cancer. *Breast Cancer Res.* **2023**, *25* (1), 104.
(10) Lan, J.; Chen, L.; Li, Z.; Liu, L.; Zeng, R.; He, Y.; Shen, Y.; Zhang, T.; Ding, Y. Multifunctional Biomimetic Liposomes with Improved Tumor-Targeting for TNBC Treatment by Combination of Chemotherapy, Anti-Angiogenesis and Immunotherapy. *Adv. Healthc Mater.* **2024**, No. 2400046.
(11) Azim, H., Jr; de Azambuja, E.; Colozza, M.; Bines, J.; Piccart, M. Long-term toxic effects of adjuvant chemotherapy in breast cancer. *Ann. Oncol.* **2011**, *22* (9), 1939−1947.
(12) Khan, A.; Khan, I.; Halim, S. A.; Rehman, N. U.; Karim, N.; Ahmad, W.; Khan, M.; Csuk, R.; Al-Harrasi, A. Anti-diabetic potential of β-boswellic acid and 11-keto-β-boswellic acid: Mechanistic insights from computational and biochemical approaches. *Biomed. Pharmacother.* **2022**, *147*, No. 112669.
(13) Ur. Rehman, N.; Khan, A.; Al-Harrasi, A.; Hussain, H.; Wadood, A.; Riaz, M.; Al-Abri, Z. New α-glucosidase inhibitors from the resins of Boswellia species with structure−glucosidase activity and molecular docking studies. *Bioorg. Chem.* **2018**, *79*, 27−33.
(14) Jamshidi-adegani, F.; Ghaemi, S.; Al-Hashmi, S.; Vakilian, S.; Al-kindi, J.; Rehman, N. U.; Alam, K.; Al-Riyami, K.; Csuk, R.; Arefian, E.; Al-Harrasi, A. Comparative study of the cytotoxicity, apoptotic, and epigenetic effects of Boswellic acid derivatives on breast cancer. *Sci. Rep.* **2022**, *12* (1), 19979.
(15) Shah, B. A.; Qazi, G. N.; Taneja, S. C. Boswellic acids: a group of medicinally important compounds. *Nat. Prod. Rep.* **2009**, *26* (1), 72−89.
(16) Hussain, H.; Ali, I.; Wang, D.; Hakkim, F. L.; Westermann, B.; Rashan, L.; Ahmed, I.; Green, I. R. Boswellic acids: Privileged structures to develop lead compounds for anticancer drug discovery. *Expert Opin. Drug Discovery* **2021**, *16* (8), 851−867.
(17) Syrovets, T.; Gschwend, J. R. E.; Büchele, B.; Laumonnier, Y.; Zugmaier, W.; Genze, F.; Simmet, T. Inhibition of IκB kinase activity by acetyl-boswellic acids promotes apoptosis in androgen-independent PC-3 prostate cancer cells in vitro and in vivo. *J. Biol. Chem.* **2005**, *280* (7), 6170−6180.
(18) Frank, M. B.; Yang, Q.; Osban, J.; Azzarello, J. T.; Saban, M. R.; Saban, R.; Ashley, R. A.; Welter, J. C.; Fung, K. M.; Lin, H. K. Frankincense oil derived from *Boswellia carteri* induces tumor cell specific cytotoxicity. *BMC Complement Altern Med.* **2009**, *9*, 1−11.
(19) Huang, M. T.; Badmaev, V.; Ding, Y.; Liu, Y.; Xie, J. G.; Ho, C. T. Anti-tumor and anti-carcinogenic activities of triterpenoid, β-boswellic acid. *Biofactors.* **2000**, *13* (1−4), 225−230.
(20) Yuan, Y.; Cui, S. X.; Wang, Y.; Ke, H. N.; Wang, R. Q.; Lou, H.-X.; Gao, Z.-H.; Qu, X. J. Acetyl-11-keto-beta-boswellic acid (AKBA) prevents human colonic adenocarcinoma growth through modulation of multiple signaling pathways. *Biochim. Biophys. Acta* **2013**, *1830* (10), 4907−4916.
(21) Agrawal, S. S.; Saraswati, S.; Mathur, R.; Pandey, M. Antitumor properties of Boswellic acid against Ehrlich ascites cells bearing mouse. *Food Chem. Toxicol.* **2011**, *49* (9), 1924−1934.
(22) Glaser, T.; Winter, S.; Groscurth, P.; Safayhi, H.; Sailer, E.; Ammon, H.; Schabet, M.; Weller, M. Boswellic acids and malignant

glioma: induction of apoptosis but no modulation of drug sensitivity. *Br. J. Cancer.* **1999**, *80* (5), 756−765.
(23) Park, B.; Prasad, S.; Yadav, V.; Sung, B.; Aggarwal, B. B. Boswellic acid suppresses growth and metastasis of human pancreatic tumors in an orthotopic nude mouse model through modulation of multiple targets. *PLoS One.* **2011**, *6* (10), No. e26943.
(24) Janssen, G.; Bode, U.; Breu, H.; Dohrn, B.; Engelbrecht, V.; Göbel, U. Boswellic acids in the palliative therapy of children with progressive or relapsed brain tumors. *Klin. Padiatr.* **2000**, *212* (04), 189−195.
(25) Streffer, J.; Bitzer, M.; Schabet, M.; Dichgans, J.; Weller, M. Response of radiochemotherapy-associated cerebral edema to a phytotherapeutic agent, H15. *Neurology.* **2001**, *56* (9), 1219−1221.
(26) Kirste, S.; Treier, M.; Wehrle, S. J.; Becker, G.; Abdel-Tawab, M.; Gerbeth, K.; Hug, M. J.; Lubrich, B.; Grosu, A. L.; Momm, F. Boswellia serrata acts on cerebral edema in patients irradiated for brain tumors: A prospective, randomized, placebo-controlled, double-blind pilot trial. *Cancer.* **2011**, *117* (16), 3788−3795.
(27) Lee, D.-H.; Kim, S.-S.; Seong, S.; Woo, C.-R.; Han, J.-B. A case of metastatic bladder cancer in both lungs treated with korean medicine therapy alone. *Case Rep. Oncol.* **2014**, *7* (2), 534−540.
(28) Togni, S.; Maramaldi, G.; Bonetta, A.; Giacomelli, L.; Di Pierro, F. Clinical evaluation of safety and efficacy of Boswellia-based cream for prevention of adjuvant radiotherapy skin damage in mammary carcinoma: a randomized placebo controlled trial. *Eur. Rev. Med. Pharmacol Sci.* **2015**, *19* (8), 1338−1344.
(29) Bini Araba, A.; Ur Rehman, N.; Al-Araimi, A.; Al-Hashmi, S.; Al-Shidhani, S.; Csuk, R.; Hussain, H.; Al-Harrasi, A.; Zadjali, F. New derivatives of 11-keto-β-boswellic acid (KBA) induce apoptosis in breast and prostate cancers cells. *Nat. Prod. Res.* **2021**, *35* (5), 707−716.
(30) Csuk, R.; Barthel-Niesen, A.; Barthel, A.; Schäfer, R.; Al-Harrasi, A. 11-Keto-boswellic acid derived amides and monodesmosidic saponins induce apoptosis in breast and cervical cancers cells. *Eur. J. Med. Chem.* **2015**, *100*, 98−105.
(31) Shamraiz, U.; Hussain, H.; Ur Rehman, N.; Al-Shidhani, S.; Saeed, A.; Khan, H. Y.; Khan, A.; Fischer, L.; Csuk, R.; Badshah, A.; Al-Rawahi, A.; Hussain, J.; Al-Harrasi, A. Synthesis of new boswellic acid derivatives as potential antiproliferative agents. *Nat. Prod. Res.* **2020**, *34* (13), 1845−1852.
(32) Jamshidi-adegani, F.; Vakilian, S.; Al-Hashmi, S.; Al-Kindi, J.; Rehman, N. U.; Al-Sinani, Y.; Ghaemi, S.; Alam, K.; Anwar, M. U.; Csuk, R.; Al-Harrasi, A. Selective anti-cancer activity against melanoma cells using 3-O-acetyl-β-boswellic acid-loaded 3D-Printed scaffold. *Nat. Prod. Res.* **2023**, *37* (12), 2049−2054.
(33) Meyiah, A.; Shawkat, M. Y.; Ur Rehman, N.; Al-Harrasi, A.; Elkord, E. Effect of Boswellic acids on T cell proliferation and activation. *Int. Immunopharmacol.* **2023**, *122*, No. 110668.
(34) Avula, S. K.; Rehman, N. U.; Khan, F.; Alam, T.; Halim, S. A.; Khan, A.; Anwar, M. U.; Rahman, S. M.; Gibbons, S.; Csuk, R.; Al-Harrasi, A. New 1H-1, 2, 3-triazole analogues of boswellic acid are potential anti-breast cancer agents. *J. Mol. Struct.* **2025**, *1319*, No. 139447.
(35) Jauch, J.; Bergmann, J. An efficient method for the large-scale preparation of 3-O-acetyl-11-oxo-β-boswellic acid and other Boswellic acids. *Eur. J. Org. Chem.* **2003**, *2003* (24), 4752−4756.
(36) Rehman, N. U.; Ullah, S.; Alam, T.; Halim, S. A.; Mohanta, T. K.; Khan, A.; Anwar, M. U.; Csuk, R.; Avula, S. K.; Al-Harrasi, A. Discovery of New Boswellic Acid Hybrid 1 H-1, 2, 3-Triazoles for Diabetic Management: In Vitro and In Silico Studies. *Pharmaceuticals.* **2023**, *16* (2), 229.
(37) Vaishnani, M. J.; Bijani, S.; Rahamathulla, M.; Baldaniya, L.; Jain, V.; Thajudeen, K. Y.; Ahmed, M. M.; Farhana, S. A.; Pasha, I. Biological importance and synthesis of 1, 2, 3-triazole derivatives: a review. *Green Chem. Lett. Rev.* **2024**, *17* (1), No. 2307989.
(38) Avula, S. K.; Rehman, N. U.; Khan, F.; Ullah, O.; Halim, S. A.; Khan, A.; Anwar, M. U.; Rahman, S. M.; Csuk, R.; Al-Harrasi, A. Triazole-tethered boswellic acid derivatives against breast cancer: Synthesis, in vitro, and in-silico studies. *J. Mol. Struct.* **2023**, *1282*, No. 135181.
(39) Gangadhar, T. C.; Vonderheide, R. H. Mitigating the toxic effects of anticancer immunotherapy. *Nat. Rev. Clin. Oncol.* **2014**, *11* (2), 91−99.
(40) Dobrzanski, M. J. Expanding roles for CD4 T cells and their subpopulations in tumor immunity and therapy. *Front. Oncol.* **2013**, *26* (3), 63.
(41) Teramoto, K.; Igarashi, T.; Kataoka, Y.; Ishida, M.; Hanaoka, J.; Sumimoto, H.; Daigo, Y. Immunotherapy. Biphasic prognostic significance of PD-L1 expression status in patients with early-and locally advanced-stage non-small cell lung cancer. *Lung. Cancer.* **2019**, *137*, 56−63.
(42) Farhood, B.; Najafi, M.; Mortezaee, K. CD8+ cytotoxic T lymphocytes in cancer immunotherapy: A review. *J. Cell. Physol.* **2019**, *234* (6), 8509−8521.
(43) Keck, S.; Schmaler, M.; Ganter, S.; Wyss, L.; Oberle, S.; Huseby, E. S.; Zehn, D.; King, C. G. Antigen affinity and antigen dose exert distinct influences on CD4 T-cell differentiation. *Proc. Natl. Acad. Sci. U.S.A.* **2014**, *111* (41), 14852−14857.
(44) Copeland, K.; Heeney, J. L. T helper cell activation and human retroviral pathogenesis. *Microbiol. Rev.* **1996**, *60* (4), 722−742.
(45) Avula, S. K.; Ullah, S.; Ebrahimi, A.; Rostami, A.; Halim, S. A.; Khan, A.; Anwar, M. U.; Gibbons, S.; Csuk, R.; Al-Harrasi, A. Dihydrofolate reductase inhibitory potential of 1H-indole-based-meldrum linked 1H-1, 2, 3-triazoles as new anticancer derivatives: In-vitro and in-silico studies. *Eur. J. Med. Chem.* **2025**, *283*, No. 117174.
(46) Finn, R. S.; Martin, M.; Rugo, H. S.; Jones, S.; Im, S. A.; Gelmon, K.; Harbeck, N.; Lipatov, O. N.; Walshe, J. M.; Moulder, S.; Gauthier, E.; Lu, D. R.; Randolph, S.; Diéras, V.; Slamon, D. J. Palbociclib and letrozole in advanced breast cancer. *New England J. Med.* **2016**, *375* (20), 1925−1936.
(47) Dang, F.; Nie, L.; Zhou, J.; Shimizu, K.; Chu, C.; Wu, Z.; Fassl, A.; Ke, S.; Wang, Y.; Zhang, J.; Zhang, T.; Tu, Z.; Inuzuka, H.; Sicinski, P.; Bass, A. J.; Wei, W. Inhibition of CK1ε potentiates the therapeutic efficacy of CDK4/6 inhibitor in breast cancer. *Nat. Commun.* **2021**, *12* (1), 5386.
(48) Samanta, S. K.; Choudhury, P.; Kandimalla, R.; Aqil, F.; Moholkar, D. N.; Gupta, R. C.; Das, M.; Gogoi, B.; Gogoi, N.; Sarma, P. P.; Devi, R.; Talukdar, N. C. Mahanine mediated therapeutic inhibition of estrogen receptor-α and CDK4/6 expression, decipher the chemoprevention-signaling cascade in preclinical model of breast cancer. *J. Ethnopharmacol.* **2024**, *319*, No. 117235.
(49) Peurala, E.; Koivunen, P.; Haapasaari, K. M.; Bloigu, R.; Jukkola-Vuorinen, A. The prognostic significance and value of cyclin D1, CDK4 and p16 in human breast cancer. *Breast Cancer Res.* **2013**, *15*, 1−10.
(50) Roy, S. K.; Kumari, N.; Pahwa, S.; Agrahari, U. C.; Bhutani, K. K.; Jachak, S. M.; Nandanwar, H. NorA efflux pump inhibitory activity of coumarins from Mesua ferrea. *Fitoterapia.* **2013**, *90*, 140−150.
(51) APEX-II, B. A., Madison, WI, USA.
(52) *SAINT V8. 40B*; Bruker AXS: Madison, Wisconsin, USA.
(53) *SADABS-2016/2*; Bruker AXS: Madison, Wisconsin, USA.
(54) Sheldrick, G. M. *Acta Crystallogr. Sect. A Found. Crystallogr.* **1990**, *46*, 467−473.
(55) Tintino, S. R.; Souza, V. C. A.; Silva, J.; Oliveira-Tintino, C. D. M.; Pereira, P. S.; Leal-Balbino, T. C.; Pereira-Neves, A.; Siqueira-Junior, J. P.; da Costa, J. G. M.; Rodrigues, F. F. G.; Menezes, I. R. A.; da Hora, G. C. A.; Lima, M. C. P.; Coutinho, H. D. M.; Balbino, V. Q. Effect of Vitamin K3 Inhibiting the Function of NorA Efflux Pump and Its Gene Expression on Staphylococcus aureus. *Membranes.* **2020**, *10* (6), 130.
(56) Ohene-Agyei, T.; Mowla, R.; Rahman, T.; Venter, H. Phytochemicals increase the antibacterial activity of antibiotics by acting on a drug efflux pump. *Microbiologyopen.* **2014**, *3* (6), 885−896.
(57) Roy, S. K.; Pahwa, S.; Nandanwar, H.; Jachak, S. M. Phenylpropanoids of Alpinia galanga as efflux pump inhibitors in Mycobacterium smegmatis mc^2 155. *Fitoterapia.* **2012**, *83* (7), 1248−1255.
(58) Moghtaderi, H.; Sepehri, H.; Attari, F. Combination of arabinogalactan and curcumin induces apoptosis in breast cancer cells

https://doi.org/10.1021/acsomega.5c01259
ACS Omega 2025, 10, 21715−21730

in vitro and inhibits tumor growth via overexpression of p53 level in vivo. *J. Biomed. Pharmacother.* **2017**, *88*, 582−594.
(59) Rahmati, M.; Zare Ebrahimabad, M.; Langari, A.; Najafi, A.; Taziki, S.; Norouzi, A.; Teimoorian, M.; Khorasani, M.; Mohammadi, S. Rosuvastatin Intervention in Patients with Chronic Hepatitis B (CHB) Expands CD14+ CD16− Classical Monocytes via Aryl Hydrocarbon Receptor (AHR). *Immuno.* **2024**, *4* (2), 159−171.
(60) Molecular Operating Environment (MOE) *2024.0601 Chemical Computing Group ULC*, 910−1010 Sherbrooke St. W., Montreal, QC H3A 2R7. 2025.

https://doi.org/10.1021/acsomega.5c01259
ACS Omega 2025, 10, 21715−21730